

ALMA MATER STUDIORUM - UNIVERSITÀ DI BOLOGNA

SCUOLA DI INGEGNERIA

DIPARTIMENTO di
INGEGNERIA DELL'ENERGIA ELETTRICA E DELL'INFORMAZIONE
"Guglielmo Marconi"
DEI

CORSO DI LAUREA MAGISTRALE IN
Ingegneria dell'Energia Elettrica

TESI DI LAUREA

in

Technological Management of Electrical Infrastructures M

FAILURE ANALYSIS OF HVDC CABLE JOINT INTERFACES

CANDIDATO

Antonio Settembre

RELATORE

Chiar.mo Prof. Andrea Cavallini

CORRELATORE

Dottor Paolo Seri

Anno Accademico
2020/2021

Contents

CHAPTER 1 INTRODUCTION	1
1.1 HVDC JOINTS	2
1.2 INTERFACE CONTACT MODEL.....	3
1.3 TANGENTIAL ELECTRIC FIELD AT INTERFACE.....	4
1.3.1 Material dependence.....	4
1.3.2 Geometry dependence	7
1.4 AIMS OF THIS THESIS	8
CHAPTER 2 SPECIMEN DESIGN.....	9
2.1 ROGOWSKI PROFILE	10
2.1.1 0.5 cm sputtered sample	11
2.1.2 1 cm specimen.....	12
2.2 MECHANICAL STRUCTURE FOR CONDUCTIVITY TESTS	13
2.3 MECHANICAL STRUCTURE FOR SPACE CHARGE TESTS.....	14
CHAPTER 3 COMSOL SIMULATIONS	15
3.1.1 Electrostatics	15
3.1.2 Electric currents	16
3.1.3 Stationary study.....	16
3.1.4 Time dependent study.....	17
3.2 CONDUCTIVITY TEST'S SIMULATIONS	17
3.2.1 3D model and COMSOL settings	17
3.3 SPACE CHARGE TEST'S SIMULATIONS.....	19
3.3.1 3D model and COMSOL settings	19
3.3.2 Space charge electrostatic simulation.....	20
CHAPTER 4 CONDUCTIVITY AND PD TESTS.....	23
4.1 CONDUCTIVITY/PRESSURE BEHAVIOUR WITH SHORT BACKING	24
4.1.1 COMSOL simulation on sputtered short backing specimen	27
4.2 CONDUCTIVITY/PRESSURE BEHAVIOUR WITH LONG BACKING.....	28
4.2.1 COMSOL simulation on sputtered long backing specimen	30

4.3	CONDUCTIVITY/PRESSURE BEHAVIOUR ON PRINTED SPECIMENS WITH SHORT BACKING	31
4.4	PARTIAL DISCHARGES	32
4.5	BREAKDOWN VOLTAGES	33
4.5.1	Broken specimens	34
4.6	“THE STEP OF DEATH”	36
CHAPTER 5	SPACE CHARGE MEASUREMENTS	39
5.1	MEASURING PROCESS	40
5.2	CHARGE AND ELECTRIC FIELD CALCULATION	41
5.3	RESULTS	42
5.3.1	Polarization under different voltages	43
5.3.2	Summary.....	44
5.3.3	Polarization and depolarization.....	45
5.3.4	Polarization and current.....	46
5.3.5	Electric field of all gaps.....	49
5.3.6	Accumulated charge over each pad.....	52
CHAPTER 6	CONCLUSIONS	55
CHAPTER 7	NARRATION OF THIS WORK	57
ACKNOWLEDGEMENTS	61
ACRONYMS	62
BIBLIOGRAPHY	63

“We are like dwarfs on the shoulders of giants, so that we can see more than they, and things at a greater distance, not by virtue of any sharpness of sight on our part, or any physical distinction, but because we are carried high and raised up by their giant size.”

Bernard De Chartres

Abstract

Negli ultimi anni l'impiego sempre più diffuso di energie rinnovabili e la necessità di una rete sempre più robusta ed interconnessa ha reso fondamentale l'impiego di linee in HVDC. All'interno di queste linee i componenti più soggetti a guasti sono giunti e terminali, i quali presentano una zona particolarmente critica: la zona interfacciale. Quest'ultima è soggetta ad un elevato campo elettrico tangenziale, il quale cambia la sua distribuzione a seconda di vari fattori.

Questo lavoro ha dunque come obiettivo quello di indagare a fondo su tale zona, per scoprirne i meccanismi di guasto e per trovare dei marker diagnostici per poter perfezionare il design dei giunti e monitorare il loro stato.

L'analisi è stata svolta utilizzando elettrodi con profilo Rogowski sputterati su dei fogli di XLPE ed inseriti in apposite presse meccaniche. Sono state svolte due tipologie di prove: una in cui si è misurata la conducibilità dei provini a vari campi elettrici e una in cui si è monitorato la carica di spazio accumulata all'interno dei provini; l'attività di scariche parziali è stata monitorata durante entrambe le prove.

Tra i possibili marker diagnostici di pre-breakdown non è stata rilevata l'utilità del monitoraggio di scariche parziali, che sembrano poter essere escluse dai meccanismi di guasto. Si nota d'altro canto un importante contributo della redistribuzione di carica all'interno del provino, che deforma notevolmente il campo elettrico al suo interno, ed è responsabile di un forte aumento di conducibilità qualche ora prima del breakdown; venendo quindi proposto come possibile parametro di monitoraggio.

Abstract

In the last years, the widespread use of renewable energy and the need for a more robust and interconnected network has made HVDC lines more and more popular. Within these lines, joints and terminals are the components most prone to failure; in these components the interfacial zone is the most critical one. The interfacial zone is subject to a high tangential electric field, and its distribution depends on many factors.

The aim of this work is therefore to investigate this zone, to discover its breakdown mechanisms and to find diagnostic markers; this will be fundamental to improve the joints design and to monitor their status.

This analysis has been carried out using XLPE sheets with Rogowski profile electrodes sputtered on it and then inserted in a particular mechanical press. Two types of tests were carried out: in the first the specimen's conductivity at various electric fields have been measured while in the second the accumulated space charge inside the specimens has been monitored; PD activity has been monitored during each of these tests.

Among the possible pre-breakdown diagnostic markers, the monitoring of partial discharges has been found to be useless, thus, they can be excluded from the possible factors of this breakdown mechanism. On the other hand, there has been a significant contribution of the accumulated space charge inside the tested specimens, which is able to significantly deform the internal electric field. Space charge has also been found to be responsible for a strong increase in the specimen's conductivity a few hours before the breakdown; thus, it has been proposed as a possible monitoring parameter.

Chapter 1

Introduction

In the last decades, the worldwide energy consumption has drastically increased and the need for a more interconnected electrical network has grown with it; nowadays, the increase of renewable energy sources, has also led to an increase of the demand for long distance connections. Due to these and for many other reasons, HVDC power transmission has become more and more attractive and competitive on the global market. In particular, HVDC cables systems are widely used to interconnect grids across the sea and to connect offshore windfarms to the power grid.

As emphasized in [1], from 2019 to 2030 *Entsoe* and *Europacable* estimates that 44 777 km of cables (of which 42 666 km in HVDC) will be needed to fulfil the need for power and reliability; so it is clear that HVDC technology will lead the future development of the power grid.

The *Entsoe* and *Europacable*'s paper, also reports that the most critical assets in HVDC systems are converting stations; however, cable failures may result in several months of downtimes and related very high costs. In cable systems (both AC and DC), the most critical parts are the joints. Indeed, as shown in Figure 1-1, about the 50% of cables systems failures are due to the joints.

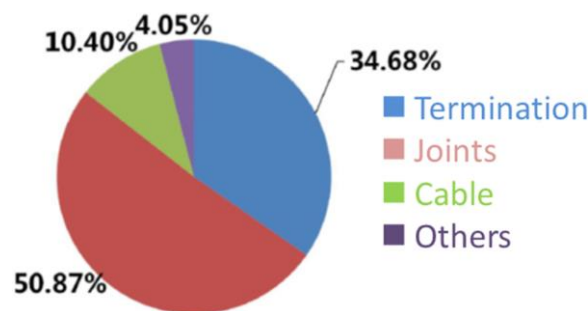


Figure 1-1 Statistical distributions of failures in 110-220kV cable systems [2],[3].

1.1 HVDC joints

As reported in [4] cable's joints can be classified in many different categories:

- Classification with respect to the installation site:
 - Factory joint: the joint is manufactured and assembled in a controlled environment;
 - Repair joint: a joint between two cables that are completed with all construction elements;
 - Field joint: a joint between two cables that are completed with all construction elements and that is installed on the field of the cable system;
- Classification with respect to the joint realization:
 - Taped joints: the insulation of the joint is realized by taping insulation strips;
 - Pre moulded joints: the insulation is elastomeric and moulded before its application on the field;
- Classification with respect to the cables system connected by the joint:
 - Straight joint: if the joint connects two cables of the same type;
 - Asymmetric joint: if the joint connects two cables with the same insulation system, but different designs;
 - Transition joint: if the joint connects two cables with different insulation systems.

A generic HVDC, a polymeric joint is made as shown in Figure 1-2:

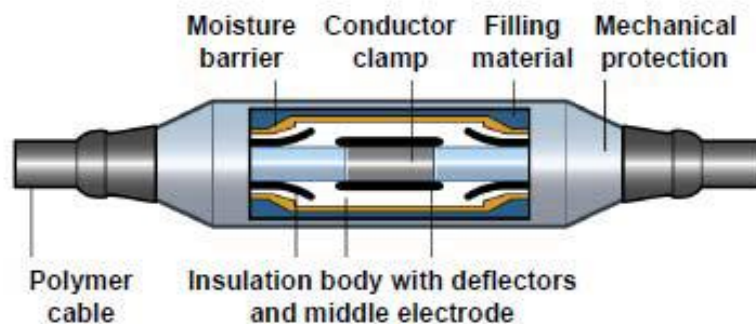


Figure 1-2 Design of a polymeric joint [3],[5]

The most critical zone in the joint is at the interface between the cable and the joint insulation right in between the inner and outer deflectors (see also Figure 2-1). This zone is particularly critical due to the tangential electric field and due to the different behaviour of the two insulations with respect to the temperature and the electric field. The interface zone is also critical because, during the joint installation, the surface may not get cleaned enough or the pressure applied to the joint may be inadequate; and this may lead to a not perfect adhesion between the surfaces.

The outer deflector (or “stress cone”) is designed to guide the electric field in order to have an adequate electric field distribution, as shown in Figure 1-3.

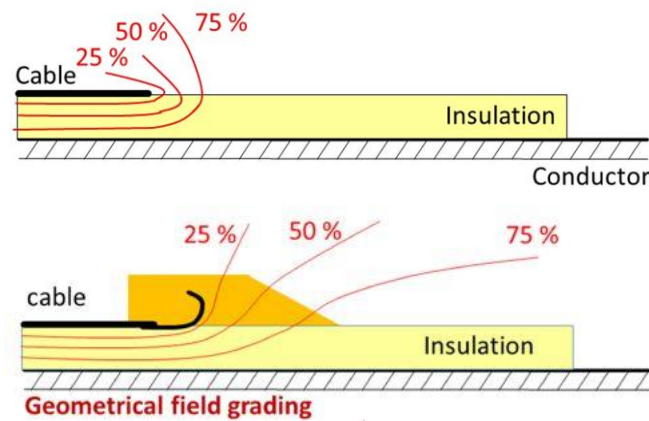


Figure 1-3 Geometrical field grading in HV terminals [3]

On the other hand, the inner HV deflector is designed to provide a smooth surface to the metallic connector in between the two conductors.

1.2 Interface contact model

Due to the material’s surface roughness, the real contact area is significantly lower than the ideal contact area. The interface contact model proposed in [6] is the Greenwood-Williamson model [7], that shows a gaussian distribution for surface’s asperities. As the pressure increases, the real contact area also increases, and with that also the breakdown strength (as shown in Figure 1-4).

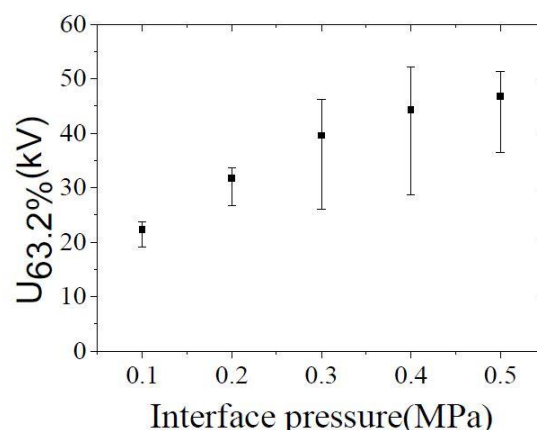


Figure 1-4 Pressure and breakdown strength (from [6])

In [6] the explanation given to this phenomena is that when the mechanical pressure increases, the contact area between the surfaces arises and the free space decreases, so that electrons will not have a lot of space to reach high kinetic energy values; moreover, the increase of the contact area, creates more surfaces on which electrical charges can adhere and weaken the electric field.

1.3 Tangential Electric field at interface

In the joint area, the electric field has also a tangential component due to the shape of the joint itself; the deflectors are carefully designed to minimize the electrical stress caused by the tangential electric field at the interface.

In Figure 1-5 different electric field distributions for a geometrical gradation joint and critical zones for different loading situations (so for different temperature gradients) are shown.

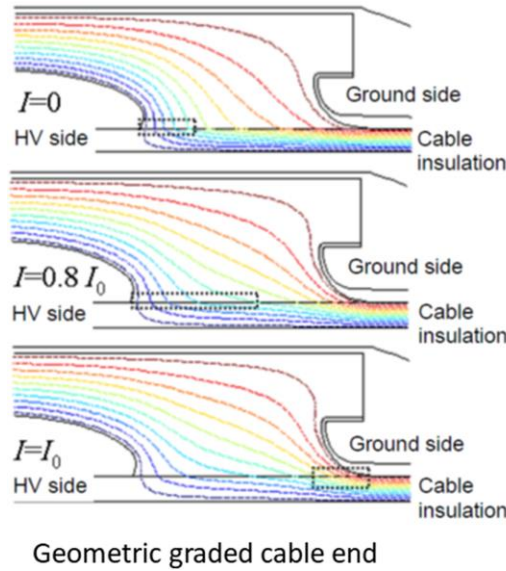


Figure 1-5 DC equipotential lines of the cable end for three different current-load cases. The dashed box shows the region of a 50% voltage drop along the interface [3],[8]

As emphasized in Figure 1-5, the maximum electric field position depends on the cable's thermal gradient: for lower loads it is nearer to the HV side, and for higher loads it is nearer to the ground side (as will be explained in more detail in sections 1.3.1 and 1.3.2 it depends also on other factors).

1.3.1 Material dependence

The electric field distribution is very different from AC to DC conditions:

In AC there is no trapped charge in the dielectric, so the electric field distribution is only determined by the cable's geometry; considering a cylindric cable, the electric field can be calculated as follows:

$$E_{AC} = \frac{V_0}{r \cdot \ln\left(\frac{r_2}{r_1}\right)} \quad (1.1)$$

In DC, the electric field distribution is determined by these equations:

$$E = -\nabla V \quad (1.2)$$

$$J = \sigma E \quad (1.3)$$

$$\rho = \nabla \cdot \varepsilon E \quad (1.4)$$

$$\nabla \cdot J = -\frac{\partial \rho}{\partial t} \quad (1.5)$$

Thus, this equation can be derived:

$$\rho = -\frac{\varepsilon}{\sigma} \frac{\partial \rho}{\partial t} + J \cdot \nabla \left(\frac{\varepsilon}{\sigma} \right) \quad (1.6)$$

That, at stationary, can be simplified by neglecting the $\frac{\partial \rho}{\partial t}$ term. So, equation (1.4) shows that E depends on ρ , and equation (1.6) shows that ρ depends on $\nabla(\varepsilon/\sigma)$; thus, if there are discontinuities in the ε/σ ratio (usually due to different materials) or if σ has a non zero gradient (usually due to the temperature gradient), there will be accumulated charge inside the dielectric volume that will modify the electric field distribution.

When a voltage V_0 is applied across two dielectrics, the charge at interface can be calculated with the Maxwell-Wagner-Sillars model as follows:

$$\rho(t) = \frac{\varepsilon_A \sigma_B - \varepsilon_B \sigma_A}{\sigma_A d_B + \sigma_B d_A} V_0 \left(1 - e^{-\frac{t}{\tau}} \right); \text{ where } \tau = \frac{d_A \varepsilon_B + d_B \varepsilon_A}{d_A \varepsilon_B + d_B \varepsilon_A} \quad (1.7)$$

Where:

- $\varepsilon_A, \varepsilon_B$ are the permittivities of the two dielectrics;
- σ_A, σ_B are the conductivities of the two dielectrics;
- d_A, d_B are the thicknesses of the two dielectrics.

In dielectric materials, conductivity depends on the temperature and on the electric field; so usually an empirical model is used to emphasize this dependency ^[1]:

$$\sigma(T, E) = \sigma_0 e^{\alpha(T-T_0) + \beta(E-E_0)} \quad (1.8)$$

Where α and β are coefficients that depends on the material and describes its dependency respectively on the temperature and the electric field; however usually α is greater than β , so in some cases and in a first approximation, β can be neglected.

¹ There are many other empirical models, such as $\sigma = \sigma_0 e^{\alpha(T-T_0)} \left(\frac{E}{E_0}\right)^\gamma$ or $\sigma = \frac{\sigma_0 e^{-\frac{G}{kT}} \sinh(cE)}{E}$, however equation (1.8) is the simplest one that shows more clearly the dependency from the electric field and from the temperature.

1.3.1.1 Conductivity dependence

As seen in the section above, the conductivity plays a fundamental role in the electric field distribution. This is true not only because of its variation with a certain temperature gradient, but also the conductivity value itself (so the value with no temperature gradient) has a key role in electric field distribution. In fact, as reported in [9], by using a material with a different conductivity, the maximum electric field value can be found on the ground or on the high voltage electrode when there is the same temperature gradient but different conductivity values.

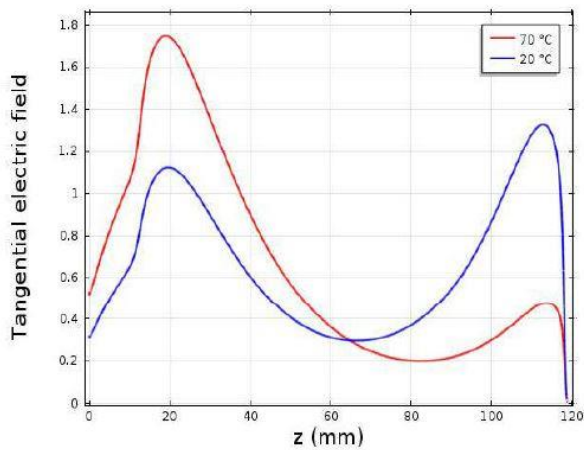


Figure 1-6 Normalized electrical field value at interface (from [9])

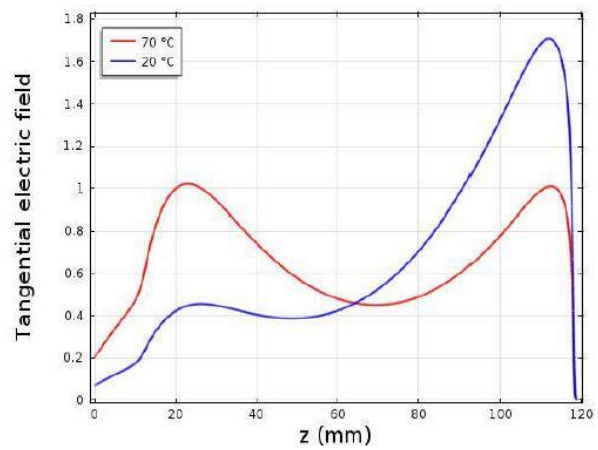


Figure 1-7 Normalized electrical field value at interface with a 10 times higher electrical conductivity (from [9])

As it can be noticed from Figure 1-6 and Figure 1-7, considering only one of the two possible conductor temperatures (so considering the same temperature gradient, but different conductivity values), the electric field distribution varies a lot when the conductivity value varies.

1.3.1.2 Temperature dependence

The electric field distribution depends on the conductivity, which in turn is affected by temperature. This section is titled “temperature dependence” since it considers the field and charge distribution in the same material under different temperature gradients. As shown in [10], the electric field distribution in an HVDC joint varies a lot when the temperature gradient arises.

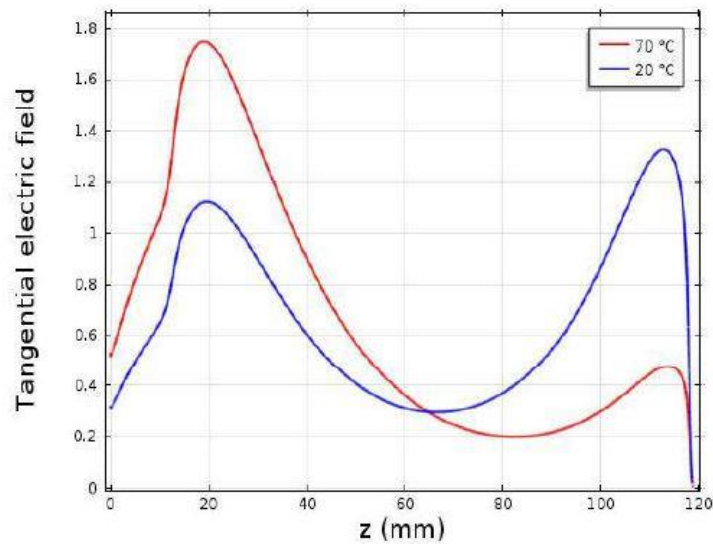


Figure 1-8 Normalized electrical field value at interface with different temperatures (0mm=ground deflector, 120mm=HV deflector) from [9].

In Figure 1-8 and also in Figure 1-5 ^[2] it is shown that the maximum electric field value can be found in different positions depending on the working temperature. Indeed, it can be found near the HV deflector in a cold joint, or near the ground deflector in a hot joint. This is due to the fact that a temperature gradient across the insulation will lead to a gradient of the permittivity/conductivity ratio, that will lead to a different field distribution.

1.3.2 Geometry dependence

The shape of the body and of the deflectors is fundamental to define the electrical field distributions at the interface. As emphasized in [11], with different designs one can obtain a maximum electrical field value on the HV or on the ground deflector as shown in the following figures.

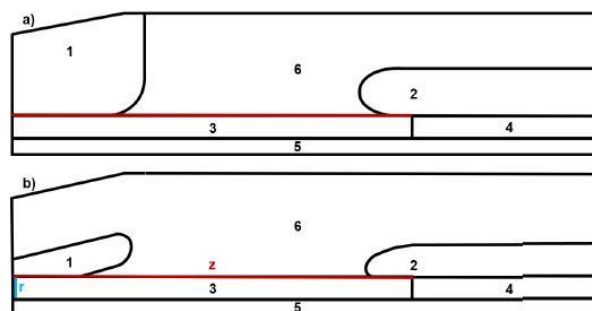


Figure 1-9 Two different geometries considered in [11]

² The figures are taken from different papers, so they are not referred to the same case, however they both shows the variation of the electrical field distribution with respect to the temperature.

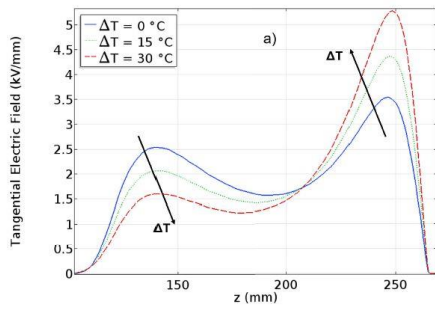


Figure 1-10 Tangential electrical field at interface with geometry (a) [11]

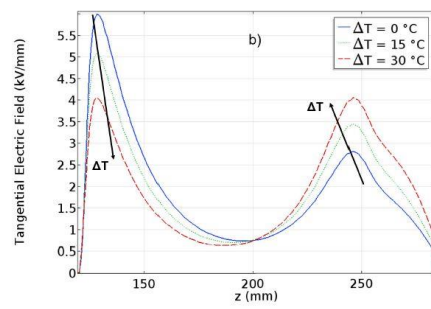


Figure 1-11 Tangential electrical field at interface with geometry (b) [11]

1.4 Aims of this thesis

As explained in the previous sections, the interfacial zone of the joint is particularly critical and its failure may lead to the damaging of the whole joint with lots of further implications. The main aim of this thesis is to investigate this phenomenon and evaluate the diagnostic markers that may indicate a joint failure.

Another goal is to evaluate the behaviour of the interfacial zone in function of the mechanical pressure applied, in order to verify if there are some particular dependencies.

Moreover, it is also important to discover which is the phenomenon that leads to the breakdown. First of all, the role of PDs. Their absence would suggest the validity of an hypothesis proposing the Coulomb force to be the main cause behind breakdown mechanisms in dielectrics.

Hence, this investigation will be carried out by means of PD detection, conduction current measurements and the evaluation of superficial charge distribution in tangentially stressed dielectric interfaces.

Chapter 2

Specimen design

As seen in section 1.3, the behaviour at the interface depends on many factors; for the purpose of this study, we decided to start with a super simplified design: the aim is to look at the behaviour of the interface under the effect of a tangential electric field, without considering the effects of temperature gradient or the effect of different materials.

To recreate the most critical interfacial zone of the joint (marked in red in Figure 2-1), we used two sheets of 0.6 mm thick XLPE arranged in multilayer configuration, as shown in Figure 2-2. One of those XLPE sheets features two sputtered Rogowski shaped electrodes, which are used to recreate a tangential electrical field.

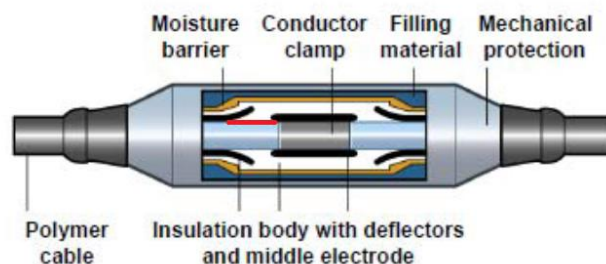


Figure 2-1 Interfacial zone (marked in red)

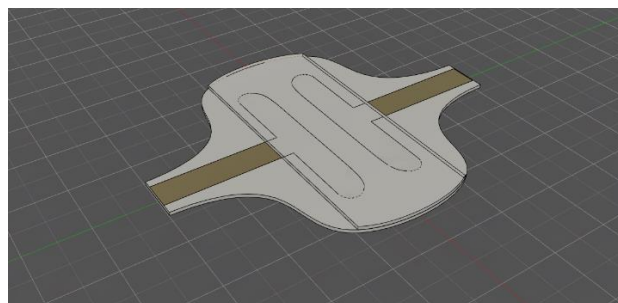


Figure 2-2 Fusion360 model of the sputtered short backing specimen

Two types of samples have been used:

- Sputtered: The electrode's profile has been sputtered in gold over the XLPE surface using an *EDWARDS-Scancoat Six Sputter Coater*.
- Printed: The electrode profile is a 0.5 mm thick semiconductive silicon.

The XLPE used has these roughness values: $R_a = 0.308 \mu\text{m}$ $R_z = 1.359 \mu\text{m}$ $R_q = 0.261 \mu\text{m}$ to simulate imperfections in the joint interface. As for the backing: a “short backing” has been used (so a backing that does not fully cover the specimen’s terminals, as shown in Figure 2-2); and a solution with a “long backing” that entirely covers the terminals was also tested.

2.1 Rogowski Profile

Since a uniform electric field distribution is only achievable with two parallel electrodes of infinite length, electrodes should be carefully designed in order to obtain the most uniform electric field distribution possible; moreover the electrodes shape should also avoid too high fields in outer regions.

The Rogowski profile lowers the edge imperfections in the electric field to obtain a more uniform distribution. As reported in [12], the equations that defines the Rogowski profile are:

$$\begin{cases} x = \frac{A}{\pi} (\Phi + e^\Phi \cos(\psi)) \\ y = \frac{A}{\pi} (\psi + e^\Phi \sin(\psi)) \end{cases} \quad (2.1)$$

In [12] it is shown that by choosing T ^[3] equal to $2d$ ^[4] the most uniform distribution of the electric field can be achieved. By considering a situation like the image charges method, the same electric field distribution can be obtained by putting two equal electrodes at the double of the distance from one to another.

Let’s define for simplicity $D = 2d$; by choosing $T = 2d$ and $\psi = \pi/2$; the Rogowski profile equation in function of D can be written as:

$$\begin{cases} x = \frac{D}{2 + \sqrt{2}} \Phi \\ y = \frac{D}{2 + \sqrt{2}} \left(\frac{\pi}{2} + e^\Phi \sin(\psi) \right) \end{cases} \quad (2.2)$$

Then, to fillet the profile to the electrode’s body, a circumference tangent to the profile in $x = 0$ with radius equal to $r = \frac{\sqrt{2}A}{\pi} = \frac{\sqrt{2}D}{2 + \sqrt{2}}$ is used. With these equations it is possible to define a Rogowski profile for every electrodes distance D . During this study, two different electrodes have been designed: one with $D = 5 \text{ mm}$ and another with $D = 1 \text{ cm}$.

³ Profile thickness

⁴ distance between the electrode and an infinite plane

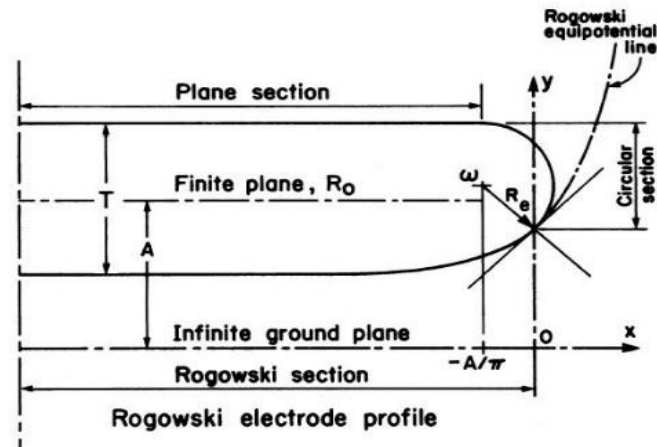


Figure 2-3 Rogowski profile (from [12])

2.1.1 0.5 cm sputtered sample

To create these samples, in order not to waste a lot of material, the XLPE sheet has been cut with a particular pattern of curves to maximize the number of samples per sheet (the cutting mask is shown in Figure 2-4); then the XLPE pieces have been cleaned with a towel and from now on they have always been handled with latex free gloves.

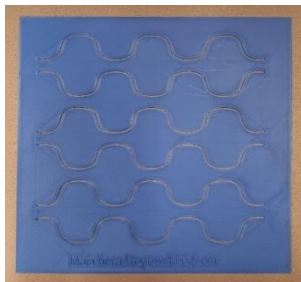


Figure 2-4 Specimen's cutting mask



Figure 2-5 3D printed 5 mm sputterer's mask

This type of specimen has been designed with $D = 5$ mm. The profile mask has been drawn using *Fusion360* and then it has been printed with a 3D printer (Figure 2-5) (the mask is 0.5 mm thick). Then the mask has been inserted inside the sputterer to impress in gold the electrodes shape on the XLPE sheet (Figure 2-6).

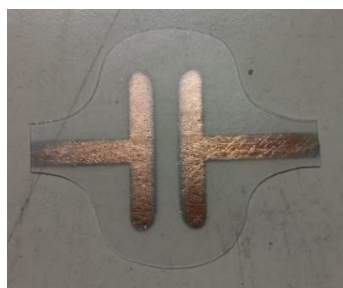


Figure 2-6 Sputtered specimen with $D = 5$ mm

2.1.2 1 cm specimen

To have a better resolution when measuring the space charge accumulated in the material (see Chapter 1), bigger electrodes have been designed (with $D = 1$ cm). Also in this case, the profile mask has been drawn using *Fusion360* and then it has been printed with a 3D printer and putted inside the sputterer.



Figure 2-7 3D printed 1 cm sputterer's mask



Figure 2-8 Sputtered specimen with $D = 1$ cm

By using a finite element calculation program (*FEMM*) the electric field distribution for this profile has been obtained (Figure 2-9).

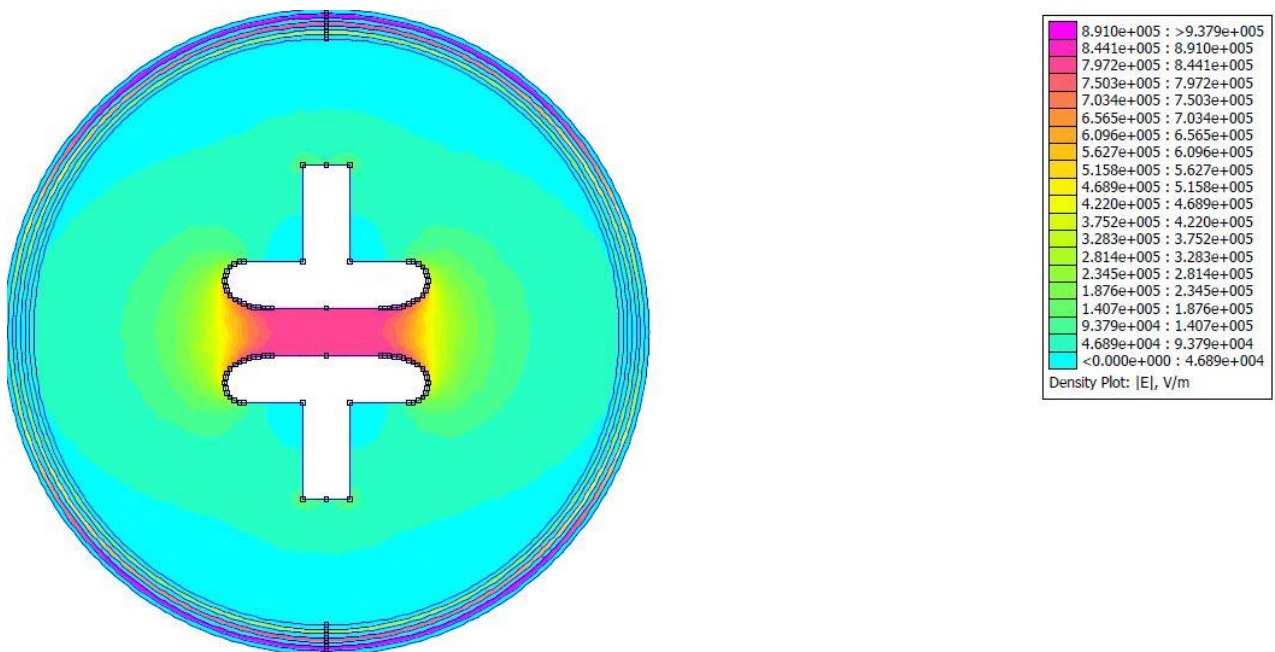


Figure 2-9 Electric field distribution in a 1 cm specimen

As shown in Figure 2-9, the electric field in the middle of the specimen is almost perpendicular and with a uniform magnitude.

2.2 Mechanical structure for conductivity tests

One of the aims of this study is to evaluate the behaviour at interface with different mechanical pressures applied on it, so a PTFE and aluminium structure has been designed to apply a certain mechanical pressure on the specimen and to keep it away from conductive parts.

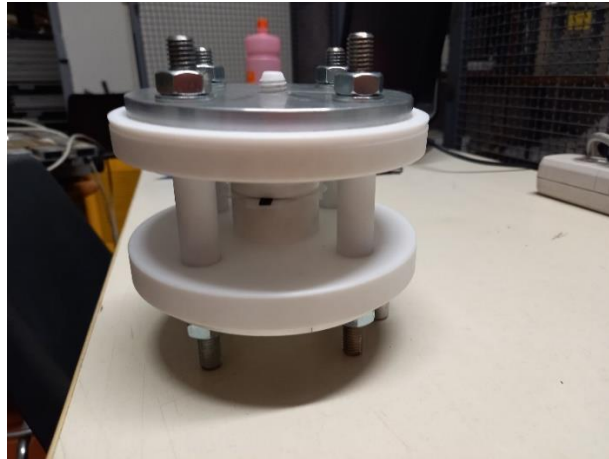


Figure 2-10 Conductivity measurements mechanical press

The structure has four bolts that are used to apply different mechanical pressures on the sample through the central cylindric pylon by means of a torque wrench.

The torque needed to tighten a bolt with a certain vertical force, can be calculated as follows [13]:

$$T = F_v \cdot \left[\frac{d_2}{2} \left(\frac{\mu}{\cos(\alpha)} + \tan(\beta) \right) + \mu_n \frac{d_n}{2} \right] \quad (2.3)$$

Where:

- μ is the friction coefficient of the threaded portion;
- μ_n is the friction coefficient of bearing portion.

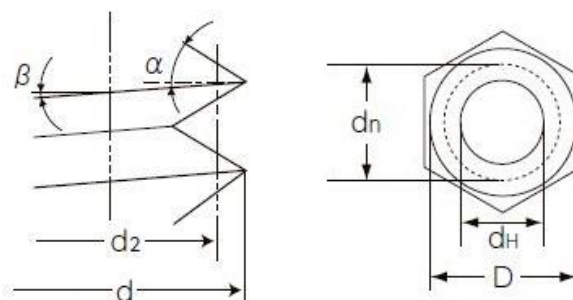


Figure 2-11 Bolt parameters

By multiplying the desired pressure for the area of contact, the vertical force needed can be obtained, and from that, the torque needed can be calculated.

Pressure on the specimen	Torque
0 bar	0 N/m
2.3 bar	0.57 N/m
3.8 bar	0.95 N/m
6 bar	1.52 N/m

Table 2-1 Pressures and torques for conductivity measurements

2.3 Mechanical structure for space charge tests

This press is wider than the previous one due to the bigger specimen used; the central cylindrical pylon is in PVC, and the other insulating material used is PMMA.



Figure 2-12 Space charge measurements mechanical press

In this case, only the central bolt is used to apply the mechanical pressure on the sample; the lateral bolts are used for structural reasons.

In this case the torque values are higher due to the highest area and to the single bolt configuration:

Pressure on the specimen	Torque
0 bar	0 N/m
1 bar	1.44 N/m
3 bar	4.31 N/m
5 bar	7.19 N/m

Table 2-2 Pressures and torques for space charge measurements

Chapter 3

COMSOL simulations

COMSOL is a simulation program that allows the user to implement many different physical models on the same 3D structure in order to study the simultaneous effect of different phenomena. When running a simulation, there are two main aspects to deal with: the physical models to implement in the simulation, and the study type (this will define in which conditions the model is evaluated).

The two physical models used in the simulations are “electrostatics” and “electric currents”; they respectively can be used to simulate the initial and the stationary electric field distribution of the model. As for the study model, mainly the “stationary” model has been used, however also two “time domain” simulations have been run to observe the evolution of the electric field when the voltage step is applied.

3.1.1 Electrostatics

“The Electrostatics interface is used to compute the electric field, the electric displacement field and potential distributions in dielectrics under conditions where the electric charge distribution is explicitly prescribed. The formulation is stationary but for use together with other physics, also eigenfrequency, frequency-domain, small-signal analysis and time-domain modelling are supported in all space dimensions.

The physics interface solves Gauss' Law for the electric field using the scalar electric potential as the dependent variable.” ^[5]

The equations implemented in the model are:

$$E = -\nabla V \tag{3.1}$$

$$\nabla \cdot D = \rho_v \tag{3.2}$$

⁵ All the sentences of these sections between the quotation marks, are reported as written in the *COMSOL* description

This physical model does not consider the space charge distribution due to the electric currents flowing in the model, so it can be used to calculate the electrical field distribution in AC conditions (which is the same as the DC in the very first instants after the HV turns on).

3.1.2 Electric currents

“The Electric Currents interface is used to compute electric field, current, and potential distributions in conducting media under conditions where inductive effects are negligible; that is, when the skin depth is much larger than the studied device. [...].”

The physics interface solves a current conservation equation based on Ohm's law using the scalar electric potential as the dependent variable.”

The equations implemented in the model are:

$$\nabla \cdot J = -\frac{d\rho}{dt} \quad (3.3)$$

$$J = \sigma E + J_e \quad (3.4)$$

$$E = -\nabla V \quad (3.1)$$

This physical model considers the currents inside of the materials and the way the distributed space charge influences the electric field distribution, so it represents the situation at time $t = \infty$, when all the charges got distributed inside the model.

3.1.3 Stationary study

“The Stationary study is used when field variables do not change over time.

Examples: In electromagnetics, it is used to compute static electric or magnetic fields, as well as direct currents. In heat transfer, it is used to compute the temperature field at thermal equilibrium. [...]. It is also possible to compute several solutions, such as a number of load cases, or to track the nonlinear response to a slowly varying load.”

This study type is used to calculate the model situation at stationary, (for $t = \infty$) so when the variables values remain almost constant with time.

In conclusion, for the model under a DC voltage, the situation at $t = 0$ is simulated with an electrostatic study at stationary, and the situation at $t = \infty$ is simulated with an electric currents study also at stationary.

3.1.4 Time dependent study

“The Time Dependent study is used when field variables change over time.

Examples: In electromagnetics, it is used to compute transient electromagnetic fields, including electromagnetic wave propagation in the time domain. In heat transfer, it is used to compute temperature changes over time. [...].”

This study type is used to obtain videos of the time evolution of the model situation; however it requires a lot of processing power, so it has been used only once to evaluate the electric field distribution in conductivity tests for a sputtered specimen.

3.2 Conductivity test’s simulations

This type of simulation has been designed to have an idea if the measured PDs during the conductivity measurements, were inside the specimen or in other parts of the measuring system. In these simulations, different types of specimens have been considered to evaluate the electric field distribution inside and outside the specimen.

3.2.1 3D model and COMSOL settings

The 3D model (Figure 3-1) considers: PTFE structure (only the central cylindric pylon), the specimen with a short backing and the electrical clamps.

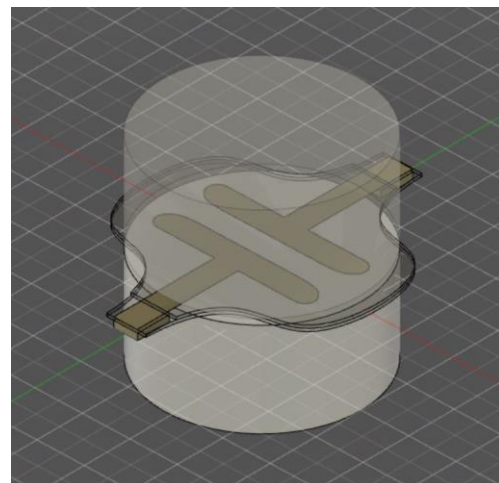
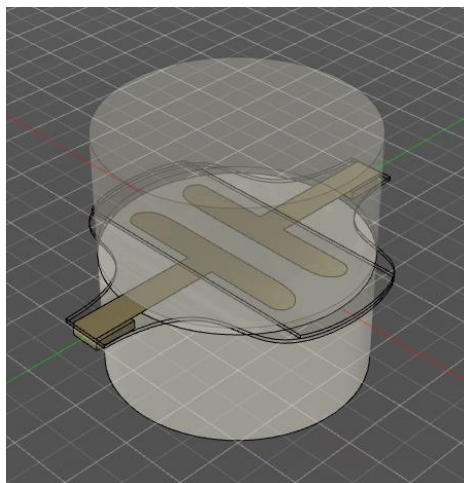


Figure 3-1 Sputtered electrodes short backing 3D model Figure 3-2 Sputtered electrodes long backing 3D model

In the simulation one electrode has been set to 20 kV and the other one is at ground potential; then the model has been inserted inside a square box of air with the boundaries at ground potential (to simulate the oven environment).

The specimen's implemented 3D models are:

- Sputtered long backing: very thin electrodes and no air gap (Figure 3-3 (a));
- Sputtered short backing: very thin electrodes and an air gap between the specimen's terminals and the PTFE structure (Figure 3-3 (b)).

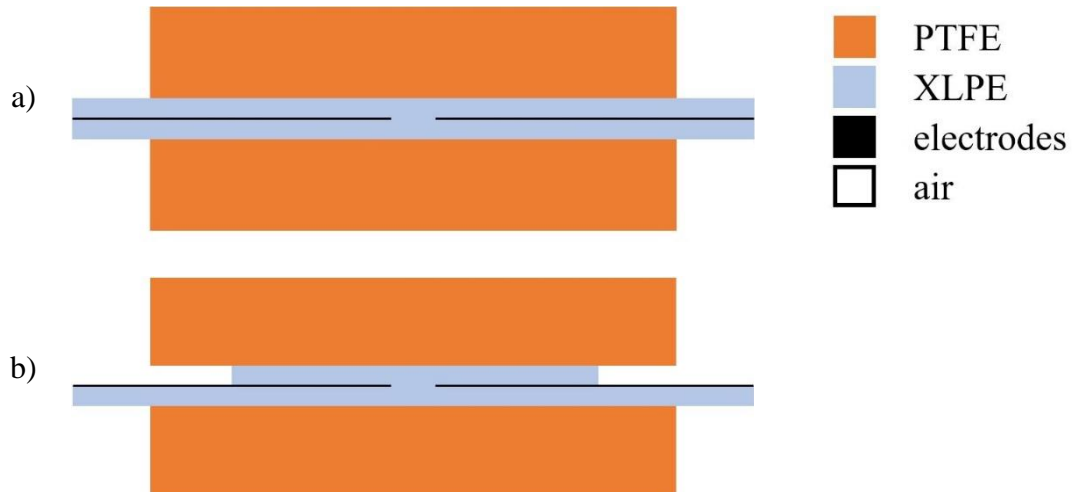


Figure 3-3 Profile view of the different electrodes models: a) Sputtered long backing, b) Sputtered short backing

3.2.1.1 COMSOL settings

In *COMSOL* there is a material library with different properties of many materials, however the conductivity values have been manually defined:

- PTFE conductivity: $5e-17$ [S/m]
- XLPE conductivity: $1e-15$ [S/m]
- Air conductivity: $1e-14$ [S/m]
- Gold conductivity: $5e7$ [S/m]

The physical models implemented in the simulations are:

- Electrostatic: to investigate the initial capacitive distribution of the electric field;
- Electric currents: to investigate the steady state condition.

The study type is stationary.

3.3 Space charge test's simulations

Due to the fact that this kind of measurement is obtained using a different specimen for each pad monitoring (see Chapter 5), the aim of this simulation is to evaluate if the obtained results are plausible or not. A time dependent electric currents study would have been interesting, but unfortunately it was a too heavy model to compute.

3.3.1 3D model and COMSOL settings

The 3D model (Figure 3-4) has been designed to simulate the mechanical structure in Chapter 1. The model presents a specimen with 1 cm gap between the electrodes, over a pcb with four metallic paths called “pads”. Each pad will assume a potential depending on the electric field distribution inside the specimen; their enumeration begins with pad 1 near the ground side and ends with pad 4 near the HV side.

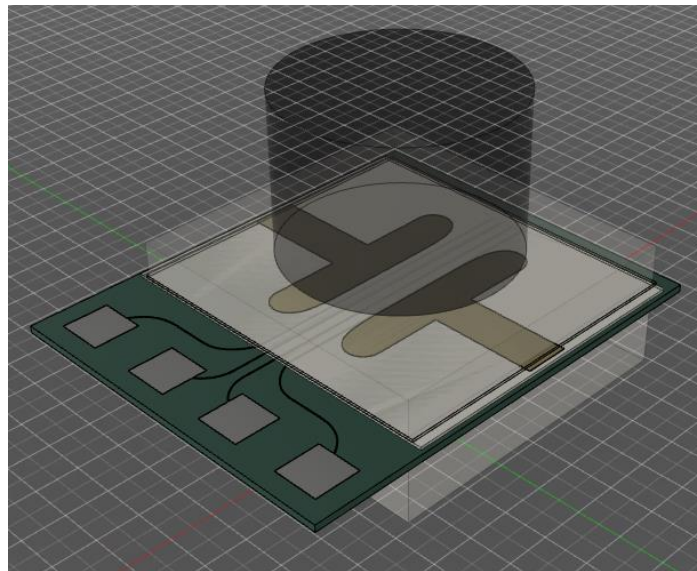


Figure 3-4 Space charge tests 3D model

The HV electrode has been set to 6 kV and the other one is at ground potential; also in this case the model has been inserted into a square box of air to simulate the oven environment.

3.3.1.1 COMSOL settings

Also in this case the conductivity values have been manually define:

- PMMA conductivity: $5e-16$ [S/m]
- PVC conductivity: $5e-16$ [S/m]
- FR4 conductivity: $1.6e-16$ [S/m]
- XLPE conductivity: $1e-15$ [S/m]
- Air conductivity: $1e-14$ [S/m]
- Gold conductivity: $5e7$ [S/m]

The physics implemented in the simulations are:

- Electrostatic: to evaluate the initial model situation;
- Electric currents: to evaluate the ending model situation.

The study type is stationary.

3.3.2 Space charge electrostatic simulation

An electrostatic stationary simulation has been run in order to have a clear view on what may happen inside the specimen and at the whole structure during the application of the DC voltage.

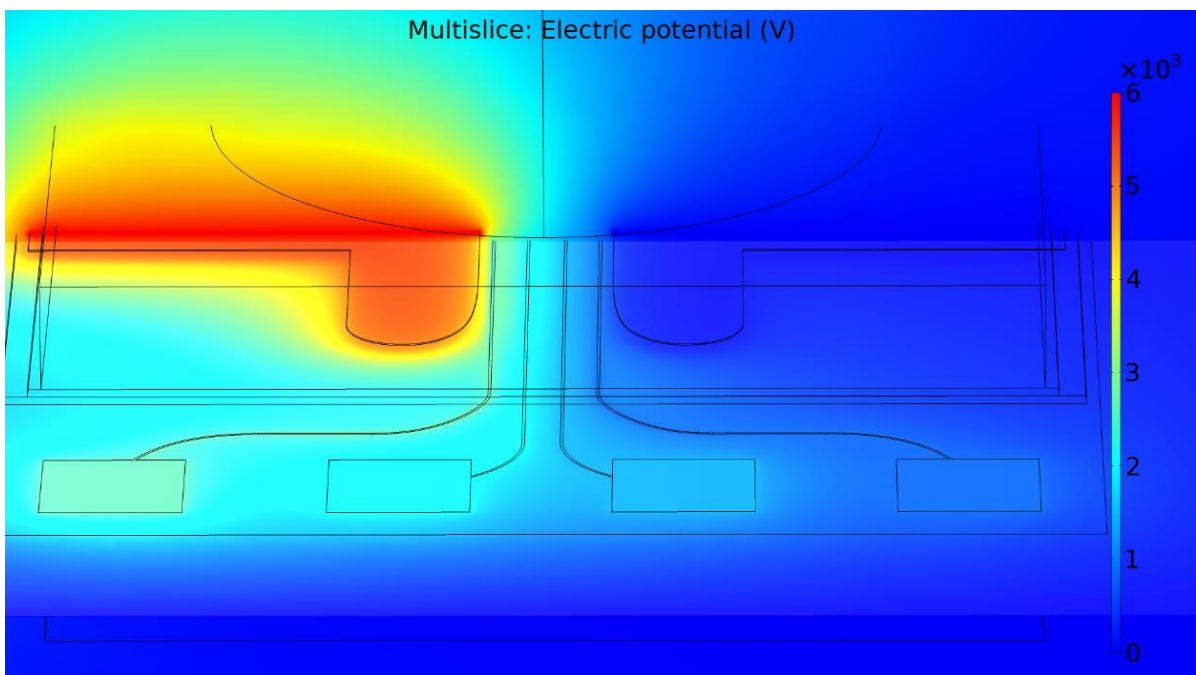


Figure 3-5 Space charge electrostatic stationary simulation (potential distribution)

As shown in Figure 3-5, the potential distribution inside the specimen increases the pads potentials so that they have increasing values, from pad 4 to pad 1.

The electric potential reached by each pad is:

Pad n.	Simulated potential	Measured potential
pad 4	2685 V	3385 V
pad 3	1926 V	2568 V
pad 2	1290 V	1602 V
pad 1	760 V	1275 V

Table 3-1 Comparison between measured and calculated potential

As expected, there is a lot of difference between the simulated potential and the measured potential at $t = 0$ (due to the fact that this is only a simulation with approximated values), however the increasing trend is confirmed by measurements (see section 5.3.2).

By looking at the electric field distribution (Figure 3-6) it can be noticed that the presence of the metallic paths influences a lot the electric field distribution, so this whole study has to be considered more from a qualitative point of view than from a quantitative one.

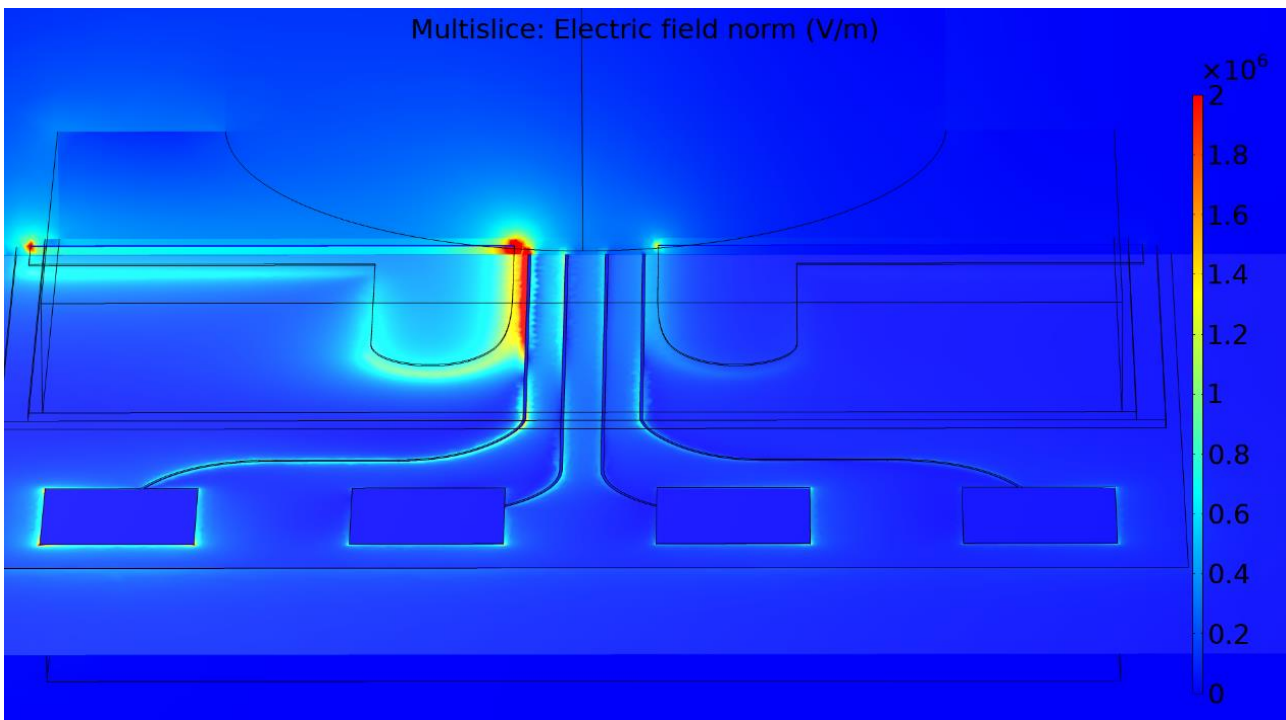


Figure 3-6 Space charge electrostatic stationary simulation (electric field distribution)

Chapter 4

Conductivity and PD tests

These measurements have been designed to: better understand the behaviour of XLPE's superficial conductivity at interface in function of the mechanical pressure applied on the sample, and to monitor the PDs situation.

To set up the measurement:

- The XLPE 5 mm sputtered specimen has been putted inside the mechanical press in Figure 2-10 and a pressure of (0 | 2.3 | 3.8 | 6 bar) has been applied by using a torque wrench.
- The oven has been set to 35°C
- A DC voltage in 8 hours duration steps of 1 kV amplitude from 1 to a maximum of 20 kV has been applied on the sample (so the electric field ranges from 0.2 kV/mm to 4 kV/mm).

During these tests the voltage has been applied with an *Heinzinger pnc-20000*, the current has been constantly monitored with a *Keysight B2980A Series Femto/Picoammeter*; and the partial discharges have been measured with a *Tektronix 5 series mixed signal oscilloscope* connected on the ground wire with a clamped *Techimp HFCT*.

The electrical circuit configuration used for the measurements is shown in figure Figure 4-1.

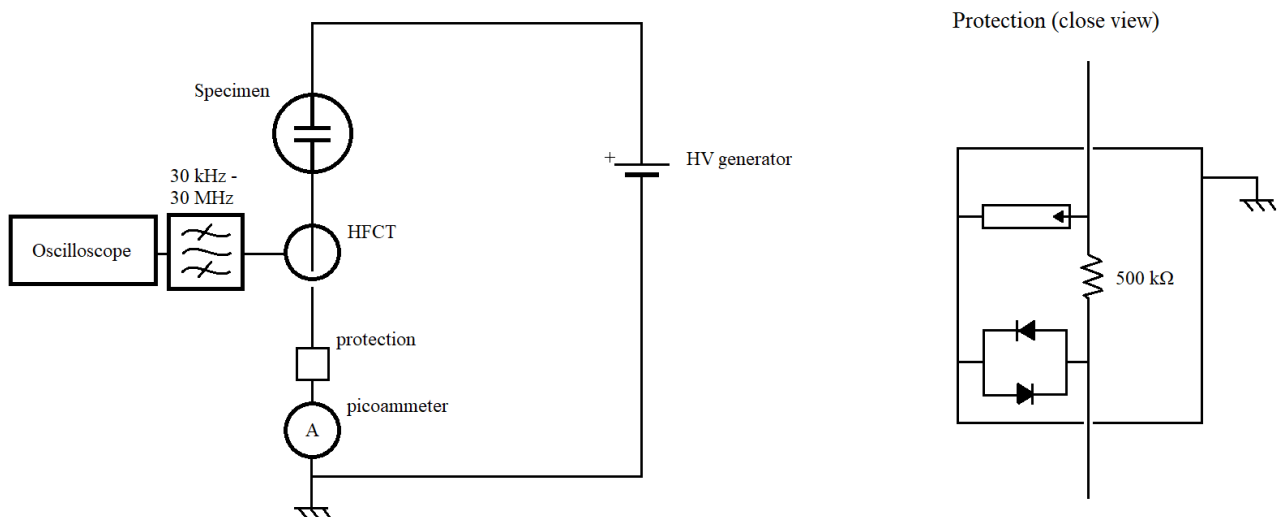


Figure 4-1 Measurement circuit



Figure 4-2 PD and Conductivity measurement system

During every measurement, the voltage has been lifted up till the specimen's breakdown, so for different pressures different specimens are used; due to this the conductivity between different pressures is not comparable.

4.1 Conductivity/Pressure behaviour with short backing

As said in the previous section, the current has been constantly monitored for the whole measuring period, then by dividing the current measured for the applied voltage and the specimen's area, Figure 4-3 can be obtained. Each plot presents many spikes and steps, they are due to the change of the applied voltage (as said in Chapter 4). In Figure 4-3 it can be seen that specimen's conductivity has a lot of fluctuations (see also section 0) and it can't be defined a trend with the applied voltage.

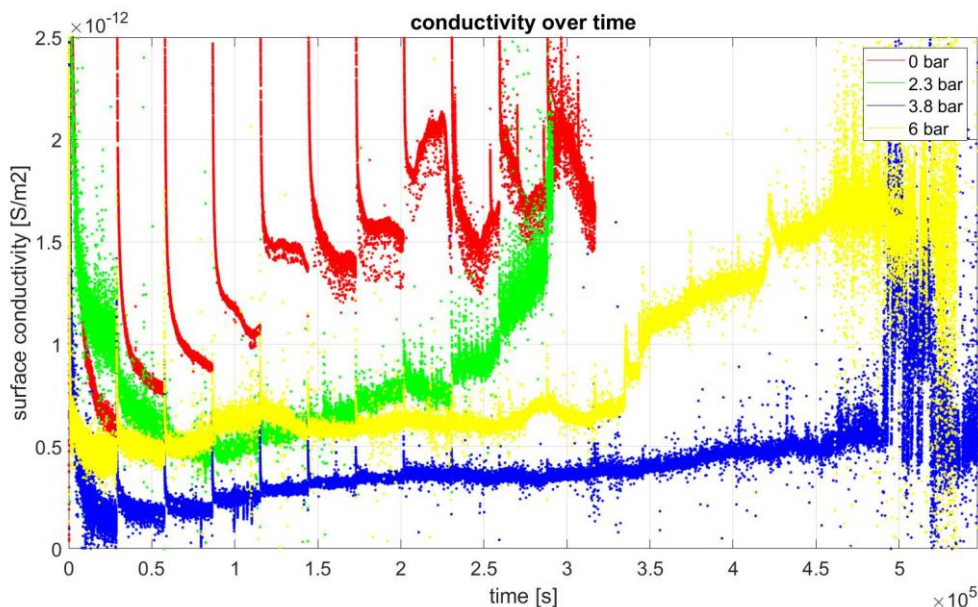


Figure 4-3 Sputtered short backing conductivity data

By calculating the mean value of the current in the last hour of each voltage step, Figure 4-4 can be obtained. Figure 4-4 shows the trend of the electrical surface conductivity as a function of the mechanical pressure applied for different electric fields.

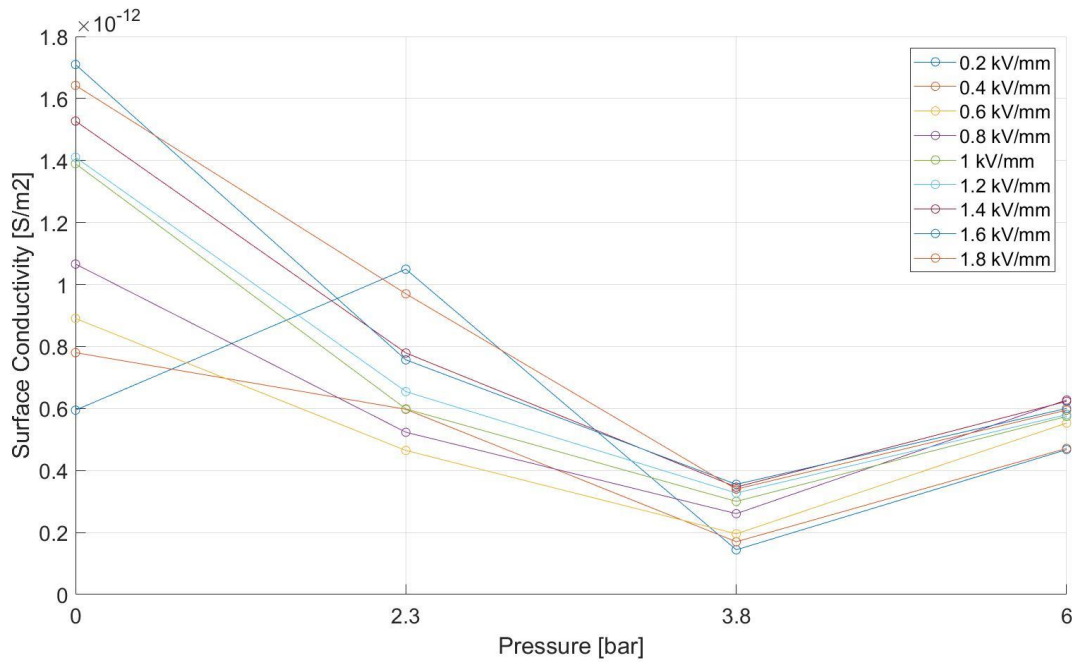


Figure 4-4 Conductivity over pressure plot at different values of electric field, sputtered electrodes, short backing

In Figure 4-5 there is a 3D representation of the plot in Figure 4-4, in order just to have a clearer view on the conductivity trends.

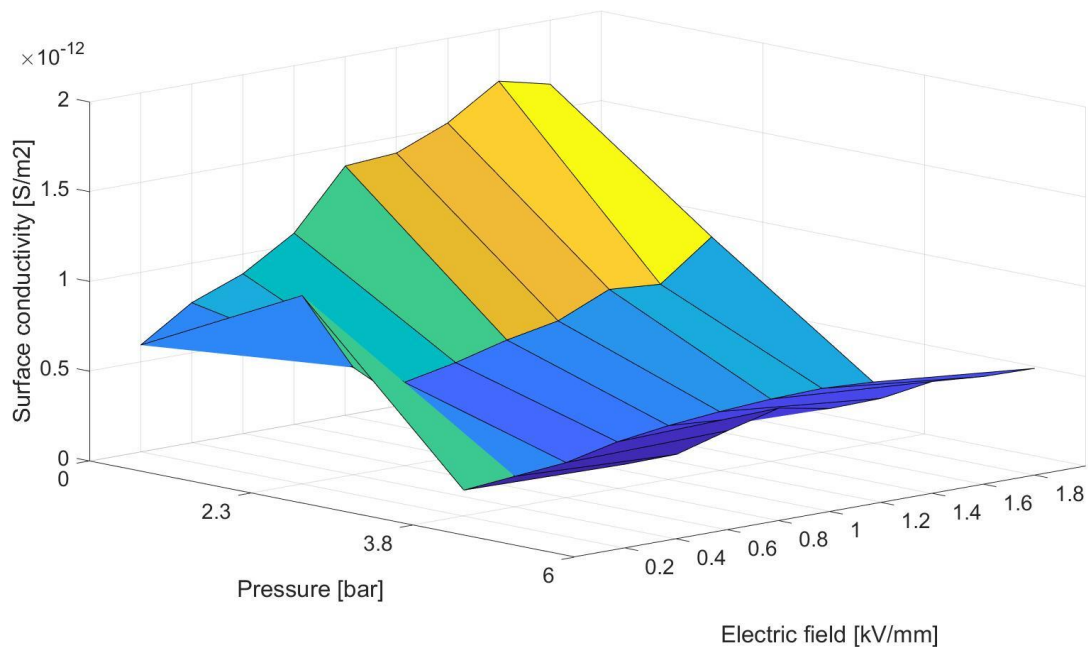


Figure 4-5 3D conductivity plot, sputtered electrodes, short backing

The main result that can be derived from these plots is that the conductivity trend presents a minimum between 3.8 and 6 bar of coupling pressure, increasing for higher pressures. This could be due to the reciprocal distance between the two surfaces: for very low pressures, there is a lot of air trapped in between, and surface conduction could play a major role; when the pressure is increased, part of the air is expelled and surface conduction might not be uniform in the specimen; by increasing pressure even more, the two surfaces will have a greater contact area (as explained in [6]) and with that also a greater number of free traps available during conduction, macroscopically reducing the mobility of free carriers.

In Figure 4-6 conductivity values at stationary have been represented with respect to the voltage and the applied pressure.

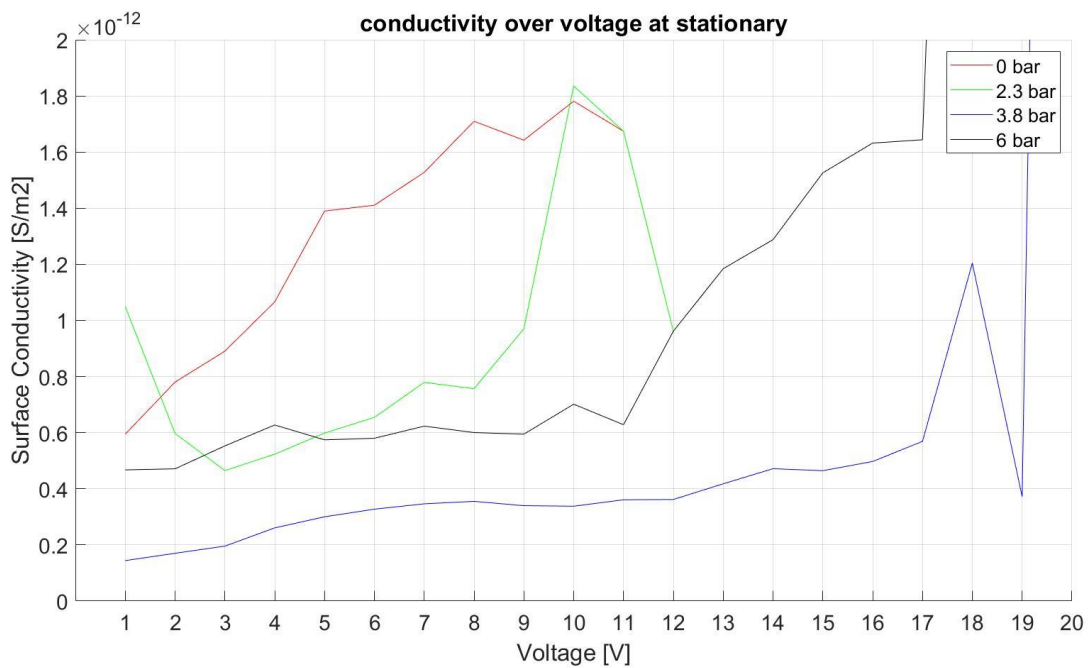


Figure 4-6 Conductivity values at stationary (short backing)

Figure 4-6 shows increasing conductivity values with respect to the applied voltage. The 2.3 bar measurement presents an initial conductivity decrease, however this initial trend is most probably due to some residual accumulated charge injected in the specimen from the metallization process.

4.1.1 COMSOL simulation on sputtered short backing specimen

This model has been designed to simulate the sputtered specimen short backing situation, due to the fact that it is not possible to use 2D electrodes (they would have been better to simulate the sputtered electrodes), the electrodes thickness has been set to 0.01 mm; this model has only two air gaps (between the specimen and the PTFE structure).



Figure 4-7 Sputtered short backing specimen, profile view



Figure 4-8 Electrostatic simulation of the short backing sputtered specimen

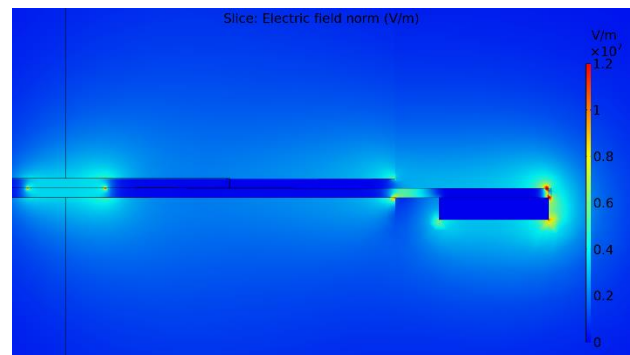


Figure 4-9 Electric currents simulation of the short backing sputtered specimen

As it can be seen from Figure 4-8, the electric field in the air gap is very high (about 4 kV/mm), so it is very plausible that corona PDs may have happened in that region; so a longer backing is needed in order to cover the entire zone between the specimen and the PTFE. Another critical zone emphasized by Figure 4-9 is the one inside the XLPE near the HV clamp, however the high electric field is located inside the XLPE, so the breakdown strength is high enough to face it.

As for the internal situation of the specimen it can be seen that initially the electric field is concentrated near the electrodes (Figure 4-8) and then, when all the charges got distributed in the volume, the electric field distribution is more uniform in the whole interfacial region (Figure 4-9).

4.2 Conductivity/Pressure behaviour with long backing

Conductivity measurements have been done also using the long backing configuration. Some measurements present a weird trend, especially the 3.8 bar measurement that shows a constant increase in conductivity with two spikes at 10 and 13 kV. During the first few voltage steps some negative conductivity values can be noticed; this may be due to some space charge that was accumulated during the specimen's metallization, not entirely discharged before the beginning of the test.

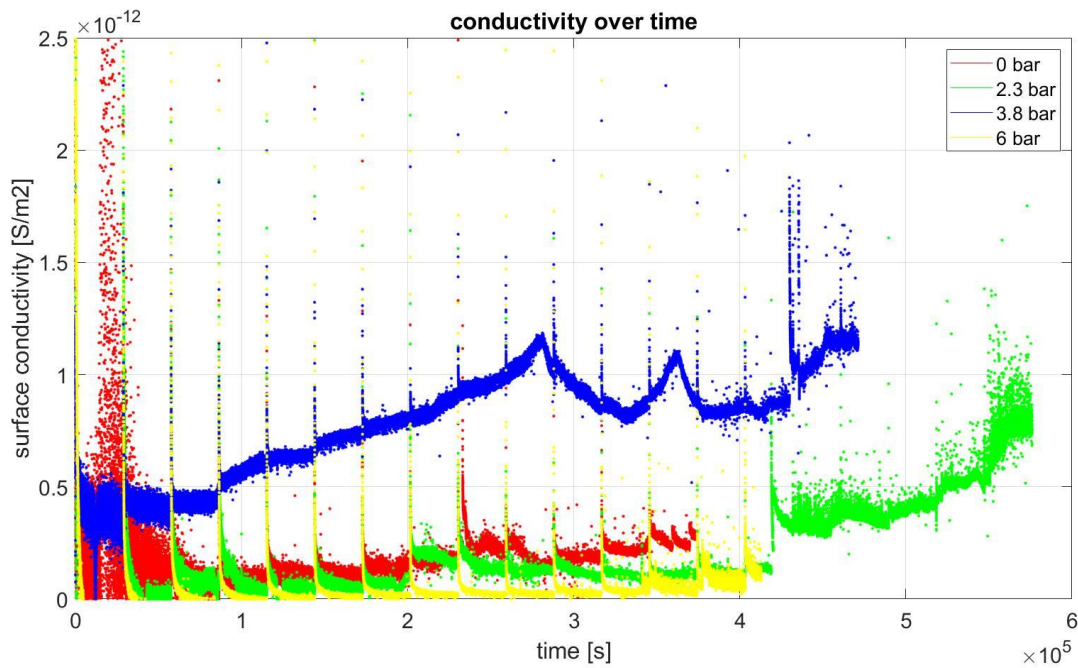


Figure 4-10 Sputtered long backing conductivity data

The 3.8 bar measurement also presents a significantly higher conductivity than the other measurements; the reason for that trend is uncertain, however these measurements are taken on a single specimen (and not as a mean value for multiple specimens), so it can also be a single case situation. The conductivity values for these specimens are a bit lower than for the short backing ones.

In the 2.3 bar measurement it can be noticed at $t = 4.1 \cdot 10^5$ s a “step of death” behaviour (see section 4.6), with the conductivity that presents a step increase in the middle of a voltage step.

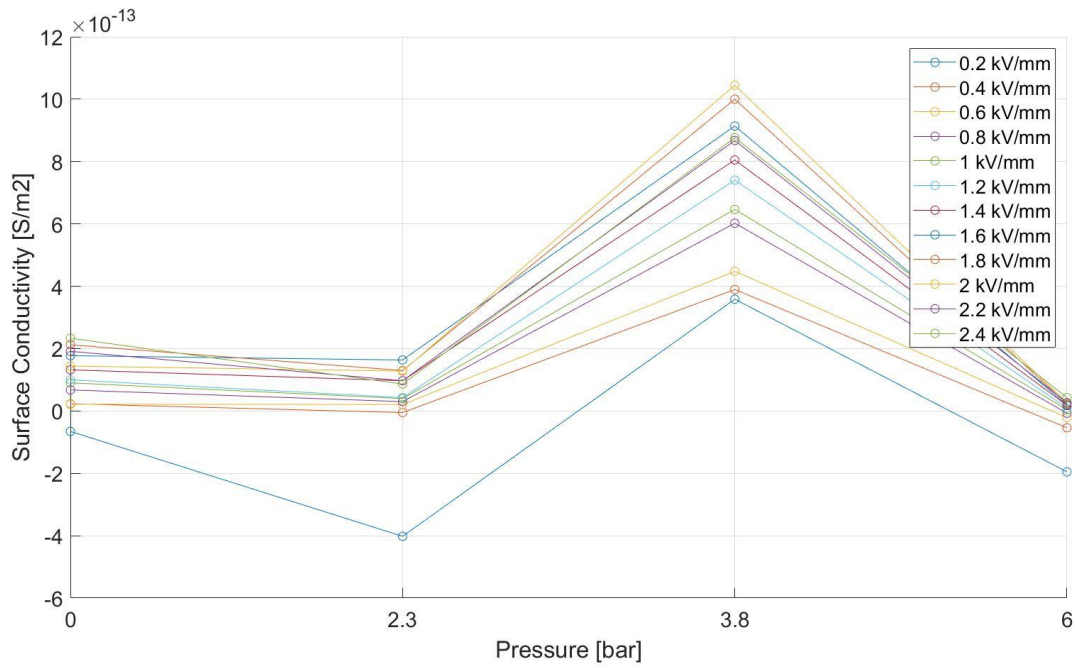


Figure 4-11 Conductivity over pressure plot at different values of electric field, sputtered electrodes, long backing

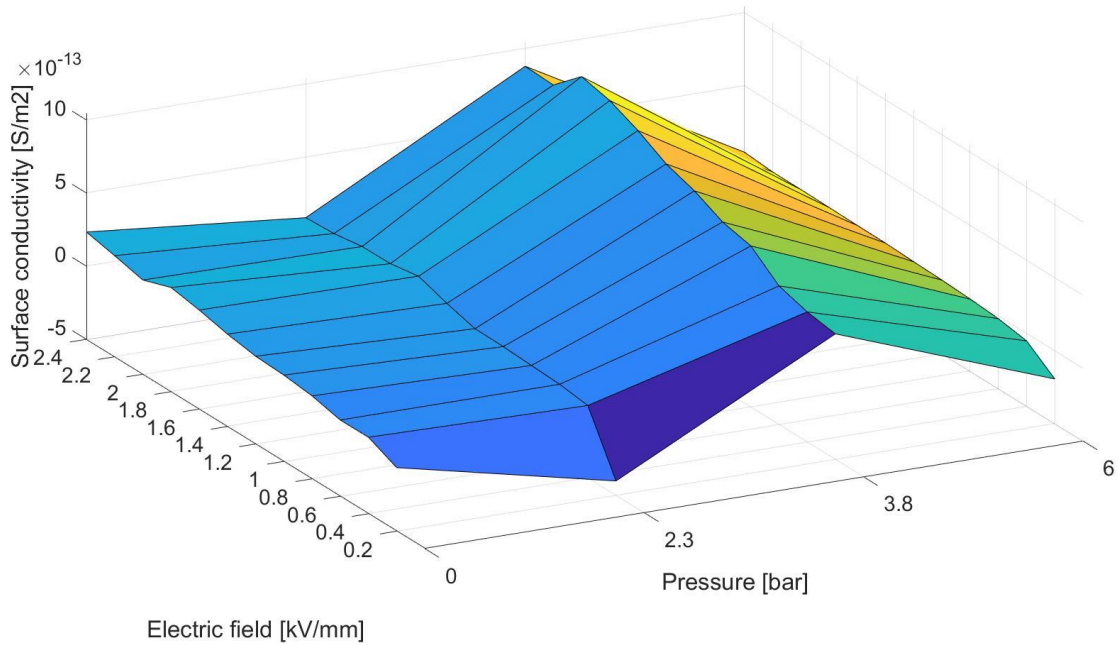


Figure 4-12 3D conductivity plot, sputtered electrodes, long backing

In complete contrast with the short backing values, in this case, the 3.8 bar measurement presents the highest conductivity values; therefore from these measurements it can't be defined a trend between surface conductivity and applied pressure.

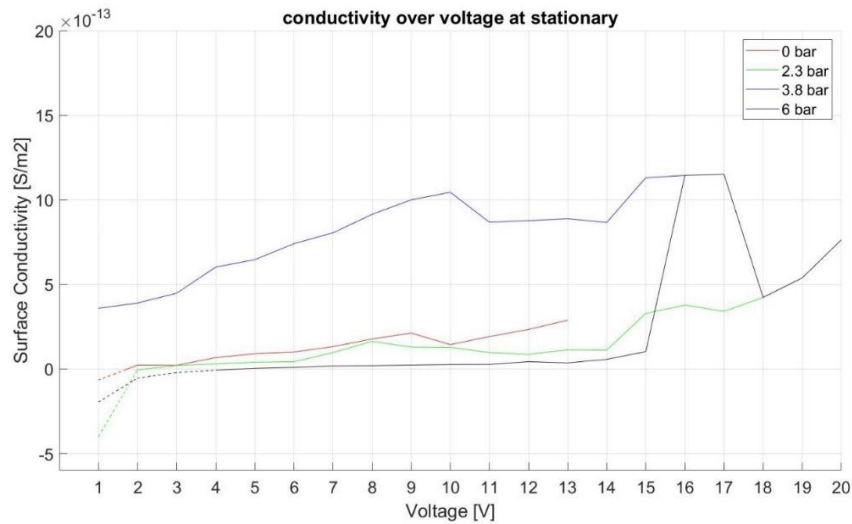


Figure 4-13 Conductivity values at stationary (long backing)

The increasing trend is confirmed; during the firsts voltage steps some negative conductivity values can be noticed, however as previously mentioned this is due to the residual charges injected by the specimen’s metallization and not entirely discharged before the beginning of the measurement.

4.2.1 COMSOL simulation on sputtered long backing specimen

Also in this case 0.01 mm electrodes have been used in the model, however now the air gaps between the electrodes and the PTFE have been covered with a longer backing.

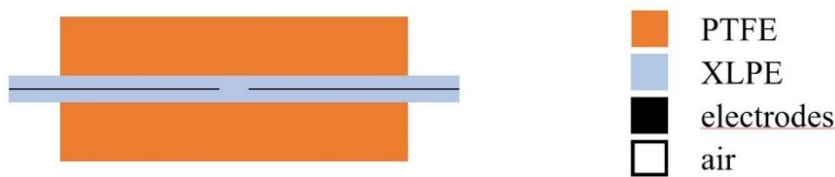


Figure 4-14 Sputtered long backing specimen, profile view

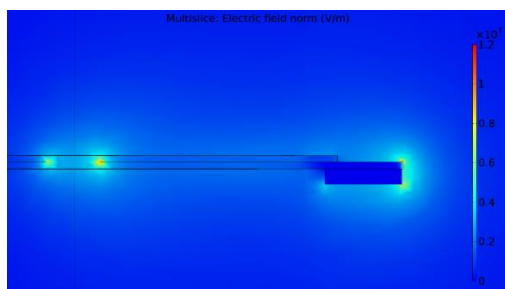


Figure 4-15 Electrostatic simulation of the long backing sputtered specimen

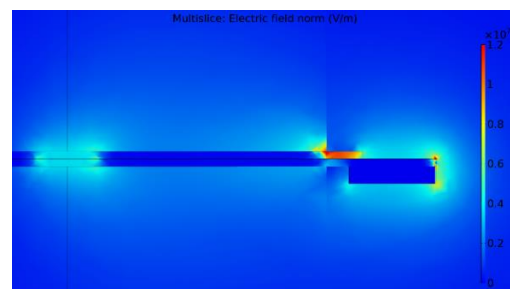


Figure 4-16 Electric currents simulation of the long backing sputtered specimen

Figure 4-16 emphasizes a critical zone near the HV electrode, where the electric field inside the specimen reaches values of about 12 kV/mm.

4.3 Conductivity/Pressure behaviour on printed specimens with short backing

Printed specimens present 0.5 mm thick electrodes; this introduces a wide air gap between the backing and the specimen.

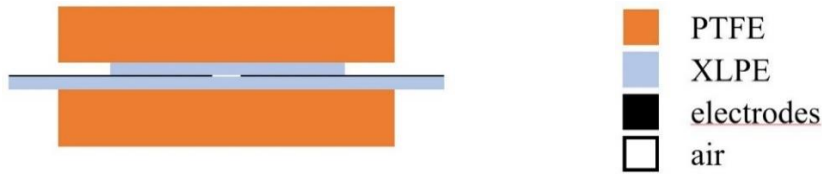


Figure 4-17 Printed short backing specimen, profile view

The wideness of this air gap is proportional to the mechanical pressure applied on the specimen; the lower is the pressure, the wider is the air gap.

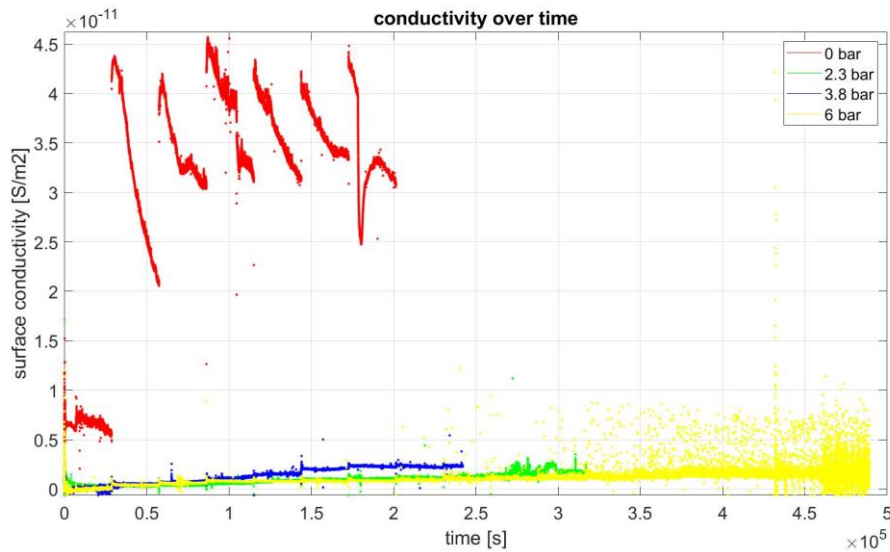


Figure 4-18 Printed short backing conductivity data

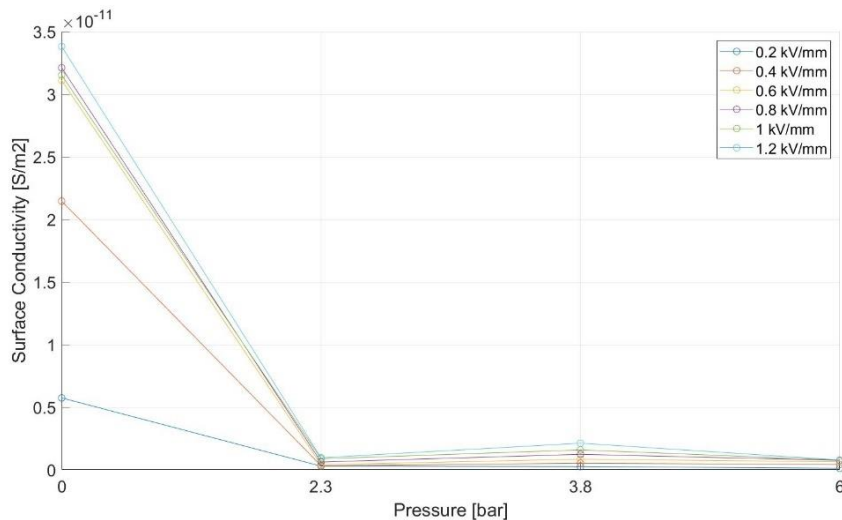


Figure 4-19 Conductivity over pressure plot at different values of electric field, printed electrodes, short backing

In Figure 4-18 and in Figure 4-19 it can be noticed that at 0 bar the specimen's conductivity is more than ten times higher than at higher pressures. This is probably due to the air gap introduced by the electrode's thickness: in fact at 0 bar the backing and the specimen's surfaces are not in contact, so the conduction effectively happens on the XLPE surfaces; by increasing the pressure the two surfaces will get in contact, therefore the conduction will be affected by this. This phenomenon does not happen with the sputtered specimens, because in that case even at 0 bar the two surfaces are in contact.

From these measurements it can be also noticed that conductivity is higher at 3.8 bar than at 2.3 bar (the same thing also happened on the sputtered long backing specimen); however this may be due to the fact that only few specimens have been tested, so there may be discrepancies between the physical alignments of the electrodes; in fact in order to define a trend it is important to have a statistically significant consistent sample.

4.4 Partial Discharges

Some PD activity was detected during the short backing tests, however also some burns on the XLPE have been found (Figure 7-4); it may suggest that the detected PD activity was not inside of the specimen but between the specimen and the PTFE. So a simulation in *COMSOL* have been run:

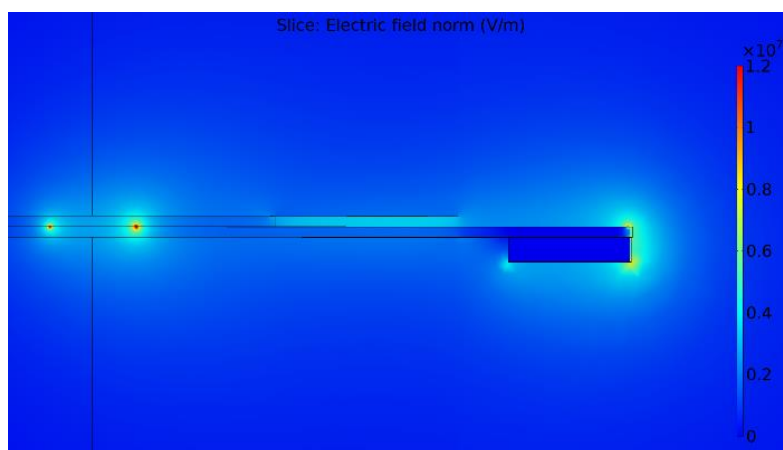


Figure 4-20 Sputtered specimen electrostatic simulation

From Figure 4-20 it can be noticed that the electric field in the air gap is very high (about 4 kV/mm), thus it is confirmed that the PD activity was not inside the specimen; hence measurements had to be repeated.

The second set of acquisitions (so the long backing ones) shows no sign of PD activity; this suggests that the measured PDs are just corona PDs, so partial discharges are not the main cause for the breakdown of the specimen interface.

4.5 Breakdown voltages

During the conductivity tests, all of the sample typologies were monitored until their breakdown. Breakdown voltages at different pressures are reported in Table 4-1.

	BD short backing [kV]	BD long backing [kV]	BD printed short backing [kV]
0 bar	11	13	7
2.3 bar	10	No BD	11
3.8 bar	No BD	16	9
6 bar	20	15	20

Table 4-1 Breakdown voltages

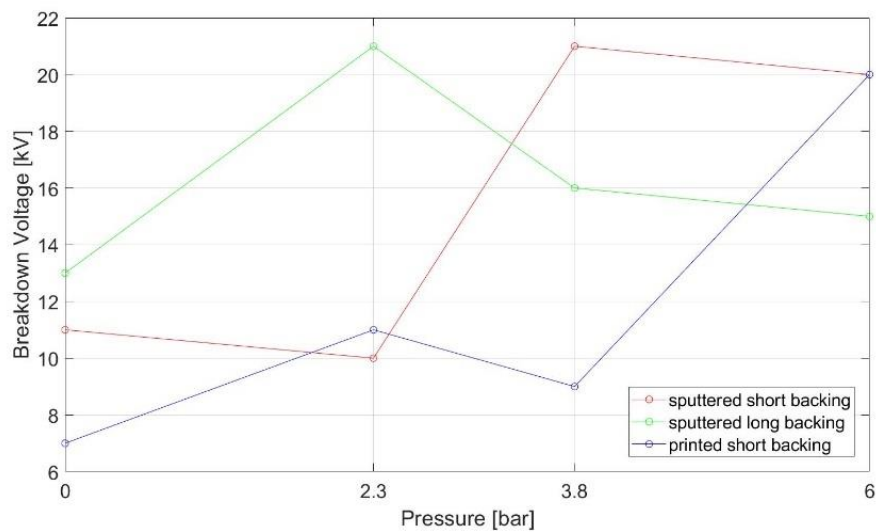


Figure 4-21 Breakdown voltages (21 kV indicates "no BD")

It can be noticed that as the pressure increases, also the breakdown strength increases, but many more measurements should be done in order to define a trend between the voltage and the pressure applied, however this topic goes beyond the aims of this thesis. A more complete study on this topic has been done in [6].

4.5.1 Broken specimens

After each breakdown, the specimens have been examined with an optical microscope; substantial differences can be noticed between the breakdown channel in sputtered or in printed specimens. The sputtered specimens do not present any visible breakdown channel. This is probably due to the vaporization of the electrode occurring as soon as the discharge happens (as it can be seen in Figure 4-22), extinguishing the arc.

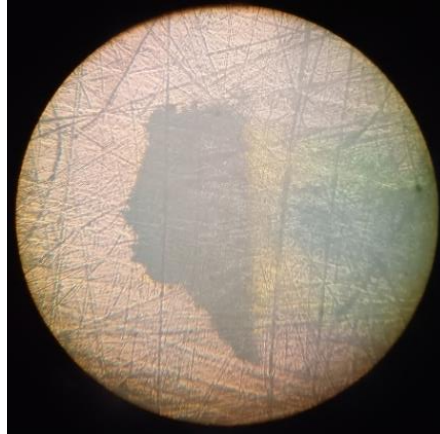


Figure 4-22 Broken sputtered specimen, this picture represents a border of a sputtered electrode that has been vaporized during the specimen's breakdown

On the other hand, printed specimens present a visible breakdown channel that clearly connects the two electrodes. From the pictures it seems that the channel does not touch the electrodes, however this is due to the deformation of the printed electrode under the mechanical pressure applied.



Figure 4-23 Printed specimen
breakdown channel

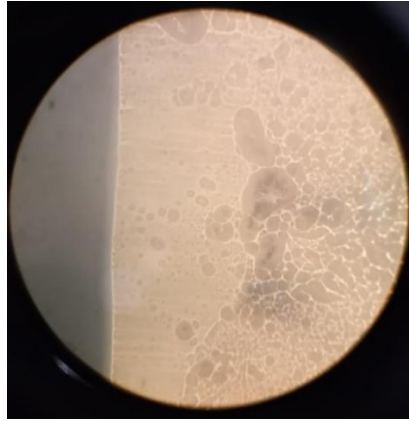


Figure 4-24 Zoom on GND electrode



Figure 4-25 Zoom on HV electrode

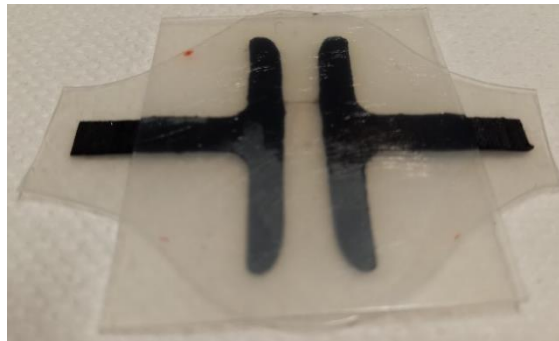


Figure 4-26 Broken printed specimen

Another printed specimen has then been examined with a Scanning Electron Microscope.

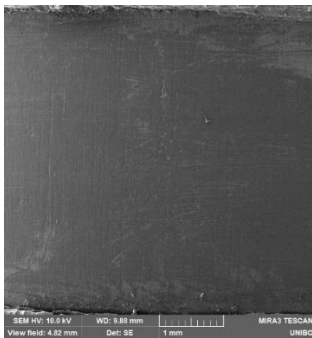


Figure 4-27 Complete breakdown
channel

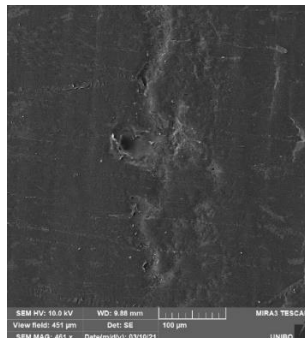


Figure 4-28 Breakdown channel
close view

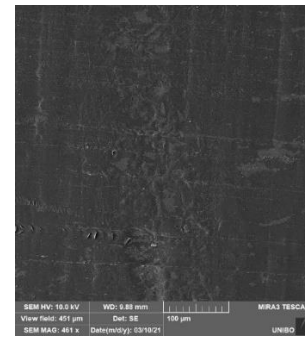


Figure 4-29 Breakdown channel
close view

4.6 “The step of death”

During many conductivity measurements, an anomalous increment in conductivity could be noticed some hours prior to the specimen’s breakdown.

In the following graphs, each colour represents a different voltage step; as mentioned, it can be noticed that sometimes, even if the voltage was constant, there has been an increment in the specimen’s current (usually it is a step increment, but sometimes also a more gradual increment). Such phenomenon was named “the step of death”.

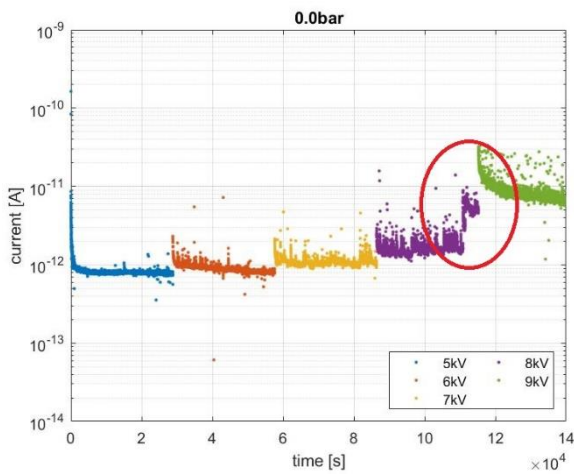


Figure 4-30 Sputtered short backing, 0 bar

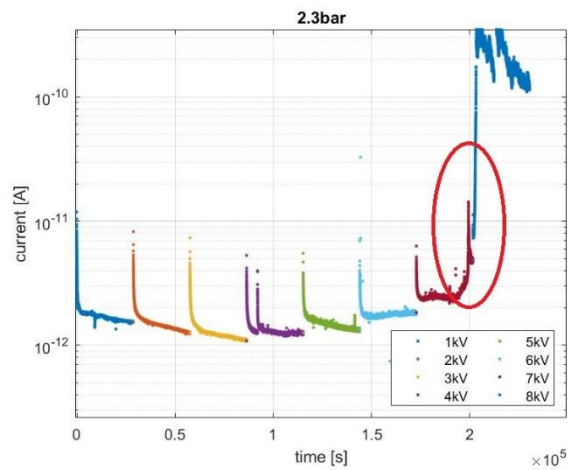


Figure 4-31 Sputtered short backing, 2.3 bar

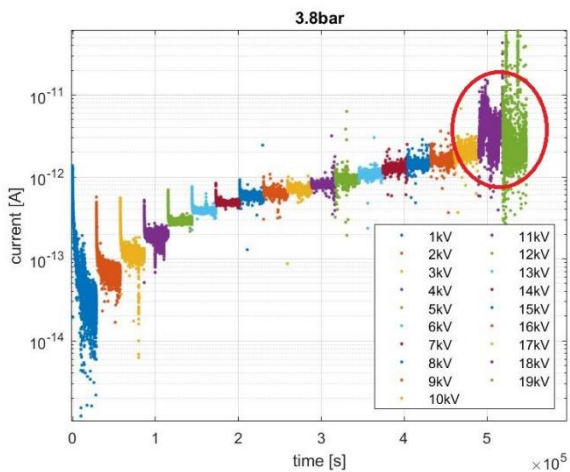


Figure 4-32 Sputtered short backing, 3.8 bar

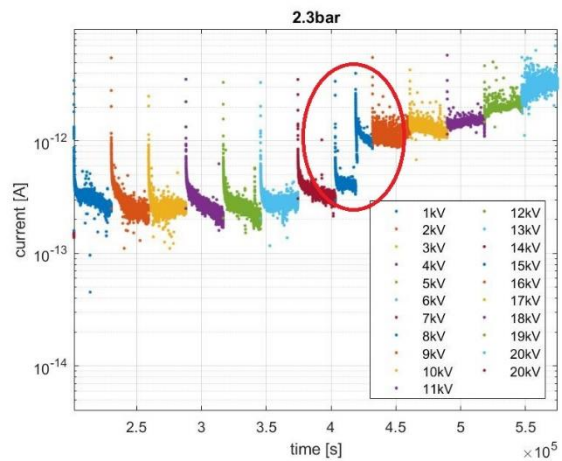


Figure 4-33 Sputtered long backing, 2.3 bar

This step increment may be due to the creation of a first breakdown channel, that however will not be conductive enough to induce a complete breakdown of the insulation; but will abruptly increase the overall conductivity of the gap.

The “step of death” surely suggests that a sudden change of charge mobility inside the specimen needs to occur before the complete breakdown process can be completed.

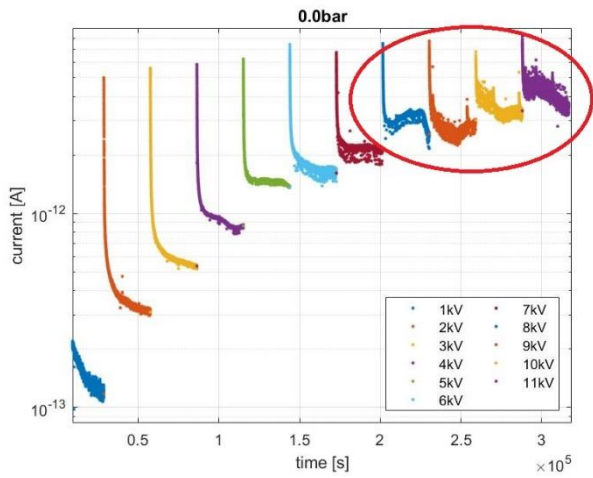


Figure 4-34 Sputtered short backing, 0 bar

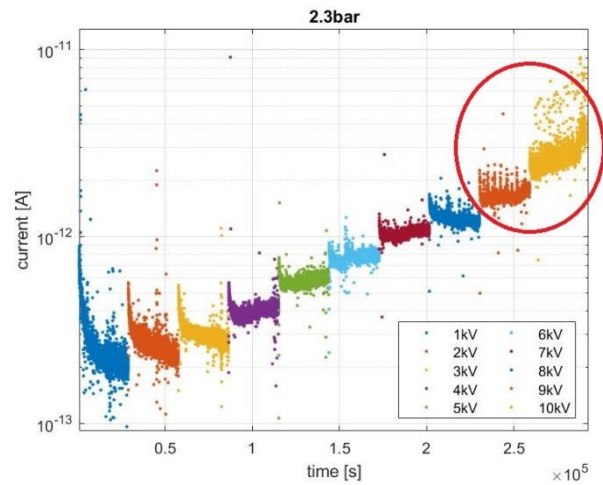


Figure 4-35 Sputtered short backing, 2.3 bar

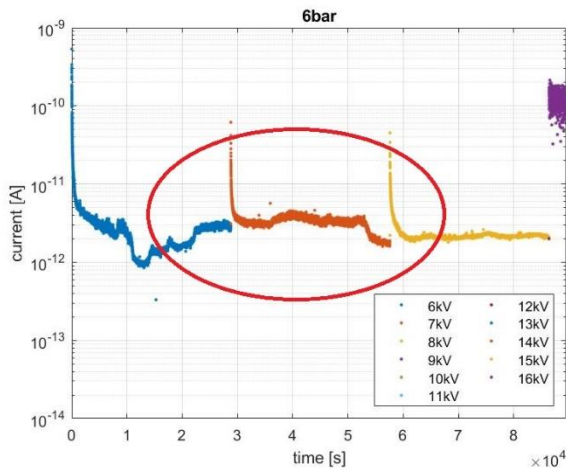


Figure 4-36 Sputtered short backing, 6 bar

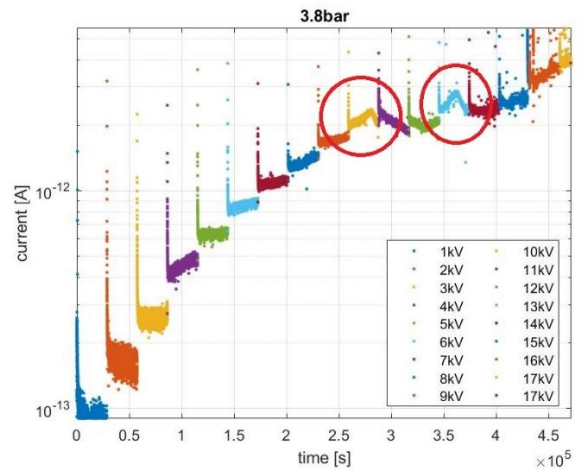


Figure 4-37 Sputtered long backing, 3.8 bar

Such phenomenon is not always clearly noticeable. As shown in Figure 4-34, Figure 4-36 and Figure 4-37, the detected currents feature very strange increasing and decreasing trends (e.g. the current shows a linear increment instead of a decrement, as in Figure 4-35).

Chapter 5

Space charge measurements

The aim of this measurement is to have a clear vision on the space charge movements and distribution during polarization and depolarization process with different pressures applied on the specimen. The press used to apply the mechanical pressure is in Figure 2-12.

In Figure 5-1 the measuring system is shown (without the used press and PD monitoring setup) and in Figure 5-2 is shown in its final configuration.



Figure 5-1 Space charge measuring system basic configuration



Figure 5-2 Space charge measuring system with PD monitoring and mechanical press

The circuit board presents four metallic paths with a floating potential, so that they will reach a certain potential that will depend on the accumulated space charge in the specimen and on the electric field applied by the HV source.

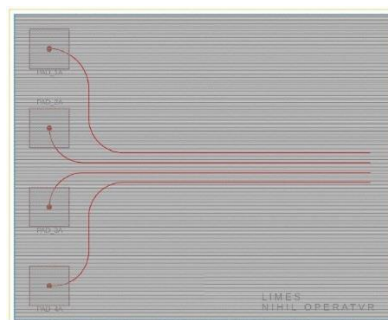


Figure 5-3 Space charge pcb's electrical scheme

The potential of each metallic path has been monitored with a *Trek model 341B electrostatic voltmeter* that has been interfaced with a computer using an *Arduino due*; the time sampling has been set to 10 Sa/s for the first 10 seconds and then lowered to 1 Sa/s for the rest of the monitoring. The monitoring has then been repeated four times (one for every metallic path) for each mechanical pressure. To maintain comparability between different tests the distance between the probe and the pcb has been regulated with a spacer keeping an air gap of 2 mm.

In Figure 5-4 it is represented the specimen situation and the names used in the following considerations.

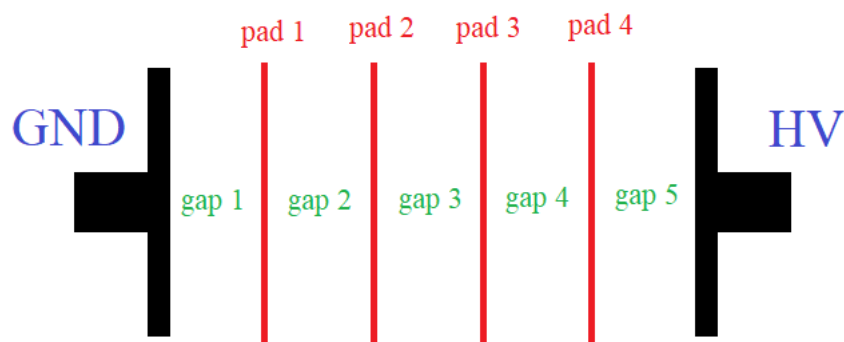


Figure 5-4 Schematic representation of the specimen (upper view)

5.1 Measuring process

To have a better resolution on the accumulated space charge, the 1 cm specimen (Figure 2-8) has been used. First of all the specimen has been sputtered, then wrapped in aluminium foil and connected to ground to remove all the space charges accumulated during the sputtering process. After a day it has been putted inside the press and manually aligned with the metallic paths in the pcb. While monitoring the electric potential of a pcb's metallic path, a 6 kV DC voltage has been applied on the specimen for at least 20 hours. After the polarization process, the HV generator has been turned off, to also measure the depolarization process. After the depolarization measurement, the specimen has been unmounted and wrapped in aluminium foil to discharge the residual space charge, mounting another specimen to proceed with the following pad. Hence, different specimens have been used for different measures, therefore discrepancies in those measurements could be expected.

Due to the fact that the electric potential measured is strongly dependent on the distance between the probe and the pcb, measurements were calibrated (as explained in section 5.3).

5.2 Charge and electric field calculation

Neglecting edge effects on the measured potential and representing the gaps between the pads as a parallel plane capacitor, the electric field in the middle of two pads can be calculated as:

$$E = \frac{V_{padR} - V_{padL}}{distance} \quad (5.1)$$

where V_{padR} and V_{padL} are the potential of the pads respectively at right and left of the selected gap. For pad 1 and pad 4 it is assumed that the electrodes are on the same plane as the pads.

Then, assuming that the charge is located only in a linear distribution over the surface of the specimen, the situation can be schematized in this way:

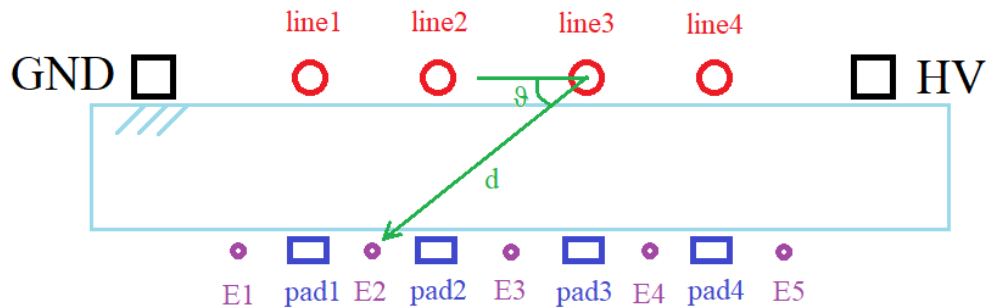


Figure 5-5 Profile view of the schematized situation

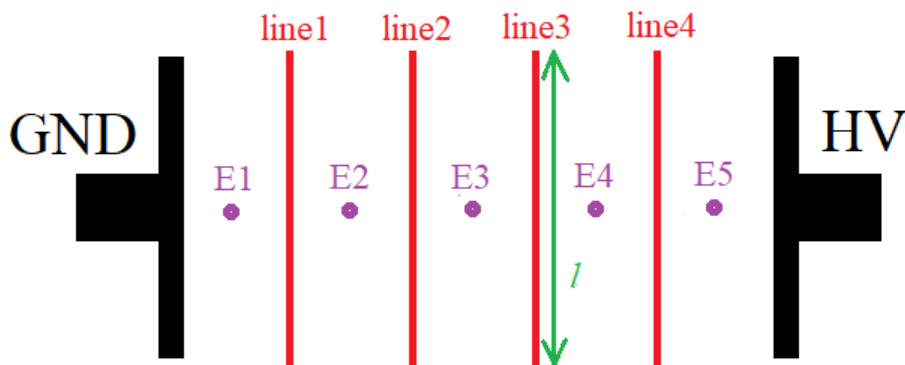


Figure 5-6 Upper view of the schematized situation

In Figure 5-5 the red circles represent the profile of the linear distribution of charges, the purple dots represent the point in which the electric field has been evaluated and the light blue area is the XLPE specimen.

The magnitude of the electric field on a perpendicular plane located in the middle of a limited linear distribution of charges, can be evaluated as:

$$E = \frac{\lambda}{2\pi\epsilon d} \cdot \frac{l}{\sqrt{l^2 + d^2}} \quad (5.2)$$

Then, by multiplying it for the cosine of ϑ (to consider only the horizontal component) and by adding the electric field generated from the HV source, it is possible to write a system of five equations in four variables (so one is redundant) and obtain the linear density of charge (λ) over each pad.

By calling:

$$a = \frac{1}{2\pi\epsilon d} \cdot \frac{l}{\sqrt{l^2 + d^2}} \cdot \cos(\vartheta) \quad (5.3)$$

Then system 5.4 can be written, where the a coefficients depends only on the geometry and nature of the material, and the E values are calculated as shown in equation 5.2:

$$\begin{bmatrix} a_{11} & \cdots & a_{14} \\ \vdots & \ddots & \vdots \\ a_{51} & \cdots & a_{54} \end{bmatrix} \cdot \begin{bmatrix} \lambda_1 \\ \dots \\ \lambda_4 \end{bmatrix} = \begin{bmatrix} E_1 \\ \dots \\ E_5 \end{bmatrix} \quad (5.4)$$

By solving this linear system, all the linear charge densities can be found; then by multiplying them for the line length (so for the specimen's width), the overall accumulated charge can be found.

5.3 Results

This section contains many different plot types and for every plot type a comparison between results at different pressures has been done.

Assuming a linear potential distribution at $t = 0$ (hence a constant electric field); these measurements can be calibrated by using a factor of correction K :

$$K = \frac{DC \text{ voltage}}{\text{number of gaps}} \cdot \frac{\text{pad number}}{\text{Initial voltage on pad } n} \quad (5.5)$$

All the plots in this section are obtained by multiplying the K factor for the measured potential values.

During all these measurements, PD activity was also monitored. Results show that no partial discharges are present during those acquisitions.

5.3.1 Polarization under different voltages

First of all the magnitude of the electric field to be applied to the specimen was chosen, since saturation of the instrument signal has to be avoided. Several tests have been run, monitoring the potential on pad 4, since it is the one expected to reach the highest values (because it is the nearest to the high voltage).

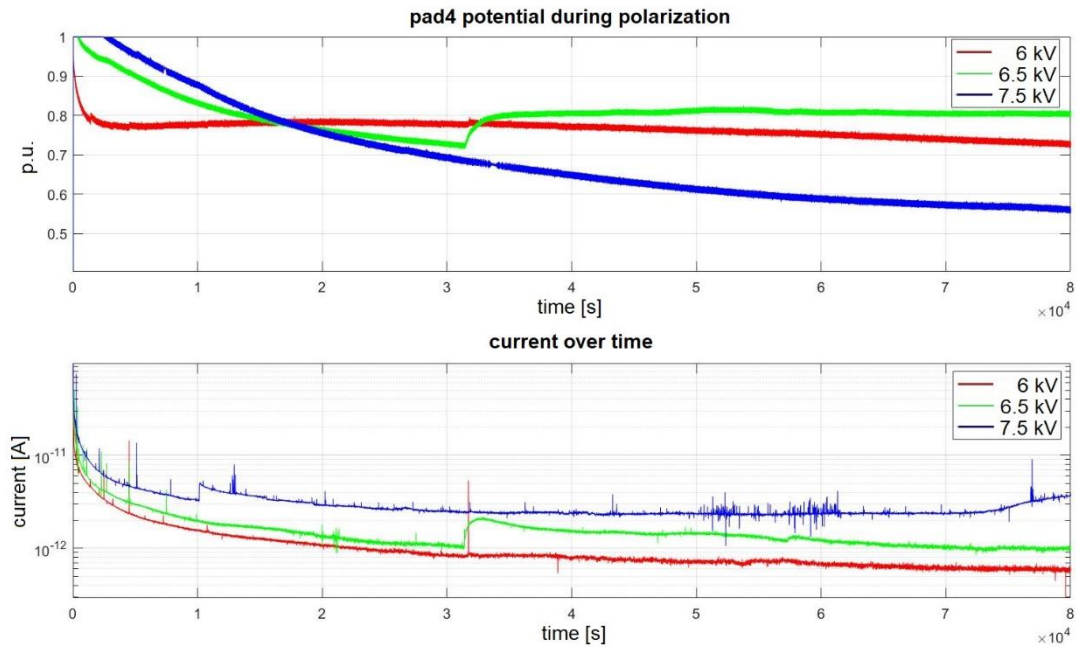


Figure 5-7 Polarization process under different voltages at 0 bar on pad 4

Figure 5-7 shows that both for 7.5 and 6.5 kV there is an initial saturation in the potential measurement, so 6 kV has been chosen for the subsequent measures.

It can also be noticed that every plot has a different time constant; this may be due to charge injection being promoted with different regimes, inducing positive oscillations on the detected current, which only apparently reaches a steady state condition much more quickly than the others. Another possibility is due to the fact that the time constant of those transients is theoretically the ratio of permittivity and conductivity of the medium. Being conductivity an increasing function of temperature and field, an increase on the latter would surely also increase the dynamics necessary to reach a steady state condition.

Another interesting phenomenon is the sudden increase both in potential and current at $t = 3 \cdot 10^4$ s (almost 8 hours) during the 6.5 kV test. Additionally, many other measurements present trend changes (usually in steepness) after almost the same amount of time.

5.3.2 Summary

In the following figures red plot represents the situation at $t = 0$ s, so it represents the voltage potential of the pads immediately after the volt on (so without any accumulated charge). Due to the fact the measurements were calibrated with the K factor, the trend is linear. On the other hand, the blue plot represents the situation after the polarization process (so exactly one instant before the volt off).

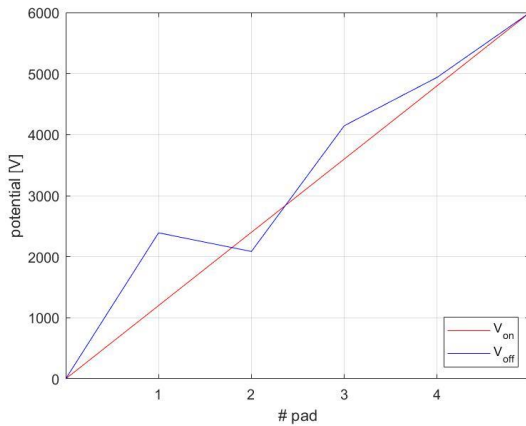


Figure 5-8 Summary situation at 0 bar

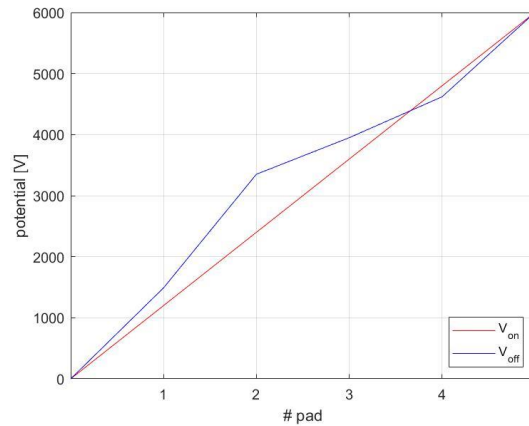


Figure 5-9 Summary situation at 1 bar

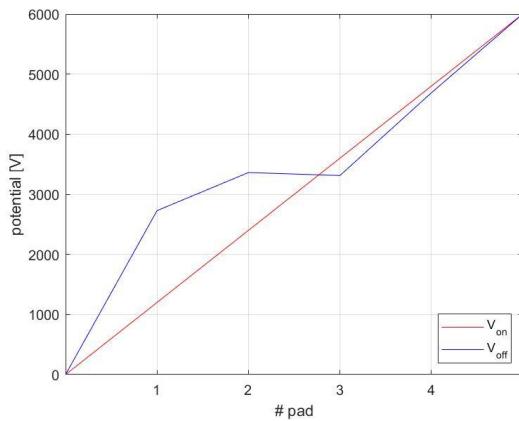


Figure 5-10 Summary situation at 5 bar

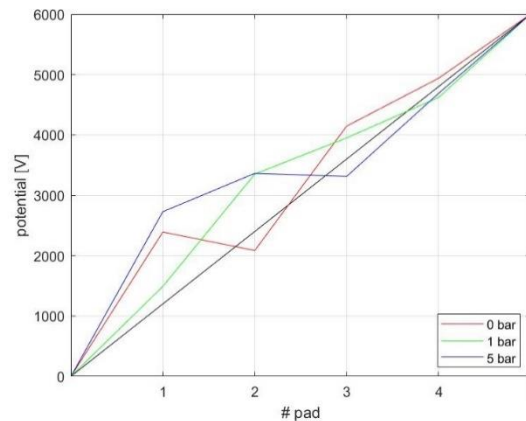


Figure 5-11 Summary situation at every pressure

In all the cases pads 1 and 2 presents the major difference between the volt on and the volt off situation; this suggests a higher field distortion near the ground electrode.

In Figure 5-8 on pads 1 and 2, and in Figure 5-10 on pads 2 and 3, it can be noticed a field inversion, however it is useful to remember that all these measurements involved a different specimen for each pad, so it is not sure that the field inversion effectively happened.

5.3.3 Polarization and depolarization

These plots show trends of the polarization and depolarization process on the same timeline; the plots also present dashed lines, which indicates the asymptotical value of the potential.

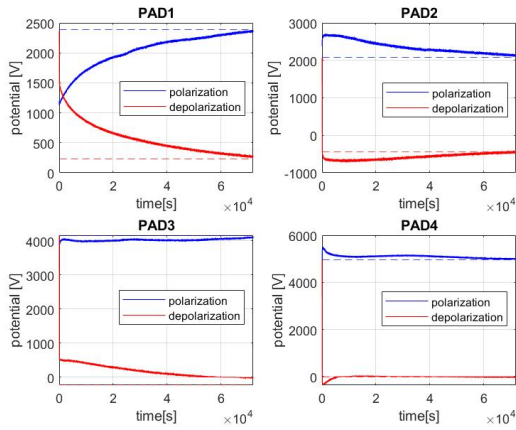


Figure 5-12 Polarization/ depolarization plots at 0 bar

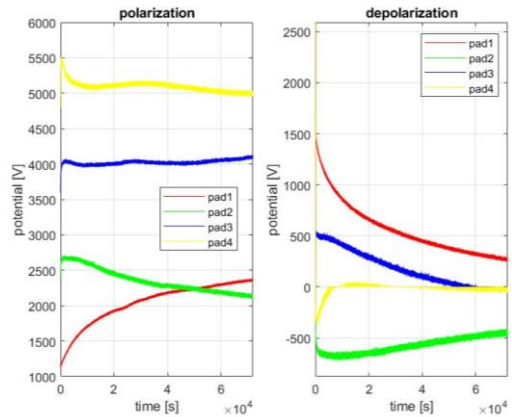


Figure 5-13 Potential of all pads at 0 bar

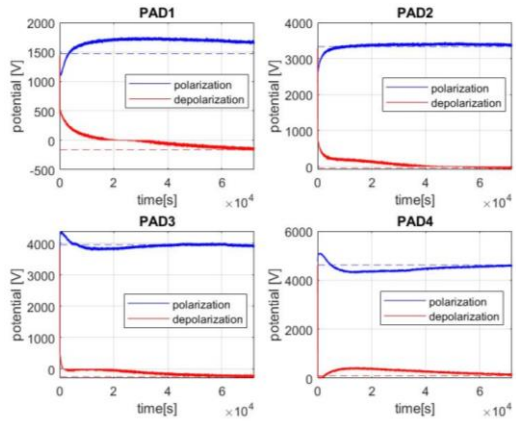


Figure 5-14 Polarization/ depolarization plots at 1 bar

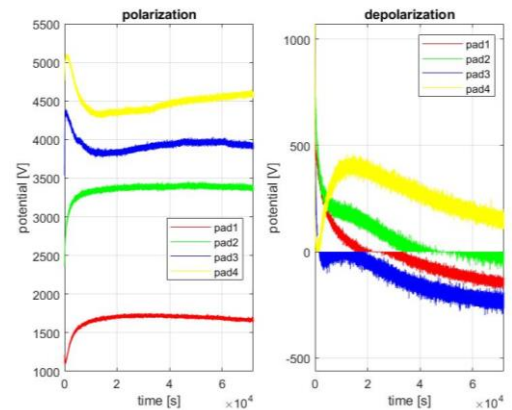


Figure 5-15 Potential of all pads at 1 bar

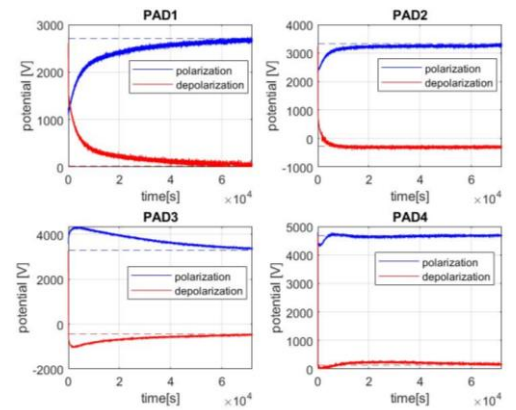


Figure 5-16 Polarization/depolarization plots at 5 bar

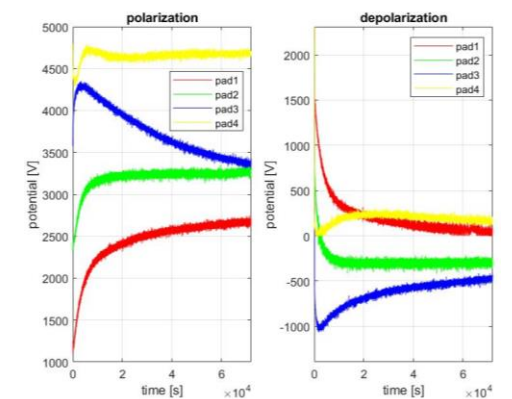


Figure 5-17 Potential of all pads at 5 bar

At 0 bar (Figure 5-12) a high amount of heterocharge ^[6] can be noticed in pad 1 and pad 4, which is slowly dissipated after $7 \cdot 10^4$ s and $0.5 \cdot 10^4$ s respectively. Also at 1 bar (Figure 5-14) an accumulation of heterocharge that got dissipated after $2 \cdot 10^4$ s can be seen on pad 1, however with the progress of the depolarization process, some negative charge flows from the adjacent pad to the ground, leading the potential to negative values. At 5 bar (Figure 5-16) a high amount of heterocharge can be found on pad 1, on the other hand, pad 4 does not present a lot of accumulated charge.

In each subplot the polarization and depolarization trends are almost symmetric, however different subplots (so different pads) presents different trends.

The potential assumed during the polarization process has different shapes on different pads, this suggest that, as it happens for space charge trapped in the bulk of a dielectric, the dynamics of the charge injected on a surface is non-uniform on the specimen, reaching a regime situation with different time constants for different pads; however a contribution to this result may also come from the different specimens used.

Charge distribution on pads 3 and 4 reaches a steady state condition in less time than on pads 1 and 2; this may suggest a lower mobility of charges near the electrodes, and a higher one in the bulk of the gap.

5.3.4 Polarization and current

These plots show both the potential value and the current injected in the specimen for each pad during the polarization process. The potential plot has then been digitally filtered with a moving average filter with a window size of 250 samples, then the derivative of the interpolation has been calculated and plotted in green to emphasize trend variations.

⁶ Heterocharge is charge accumulated near to an electrode with a potential of opposite sign; on the other hand, homocharge is an accumulation of charge with the same sign. Globally, heterocharge is usually more dangerous than homocharge, since it leads to a local increase of the electric field. Heterocharge accumulation inside the specimen can be noticed whenever a potential increase can be found at pad 1 (near the ground electrode), or a decrease on pad 4 (near to the positive HV electrode).

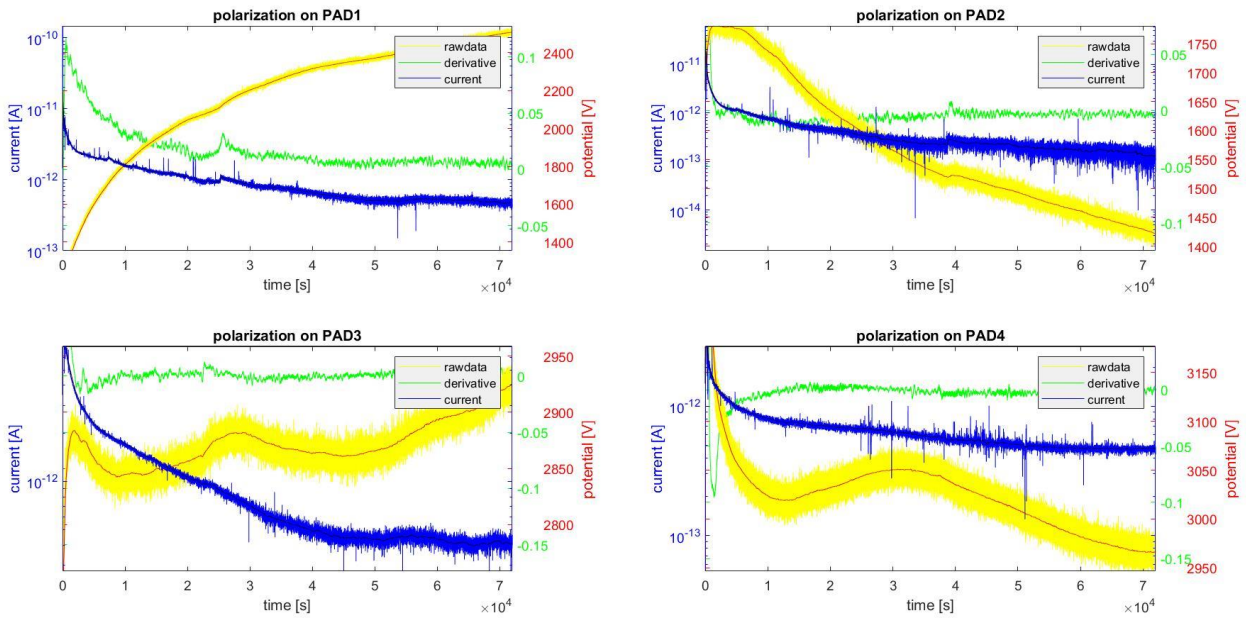


Figure 5-18 Polarization and current plots at 0 bar

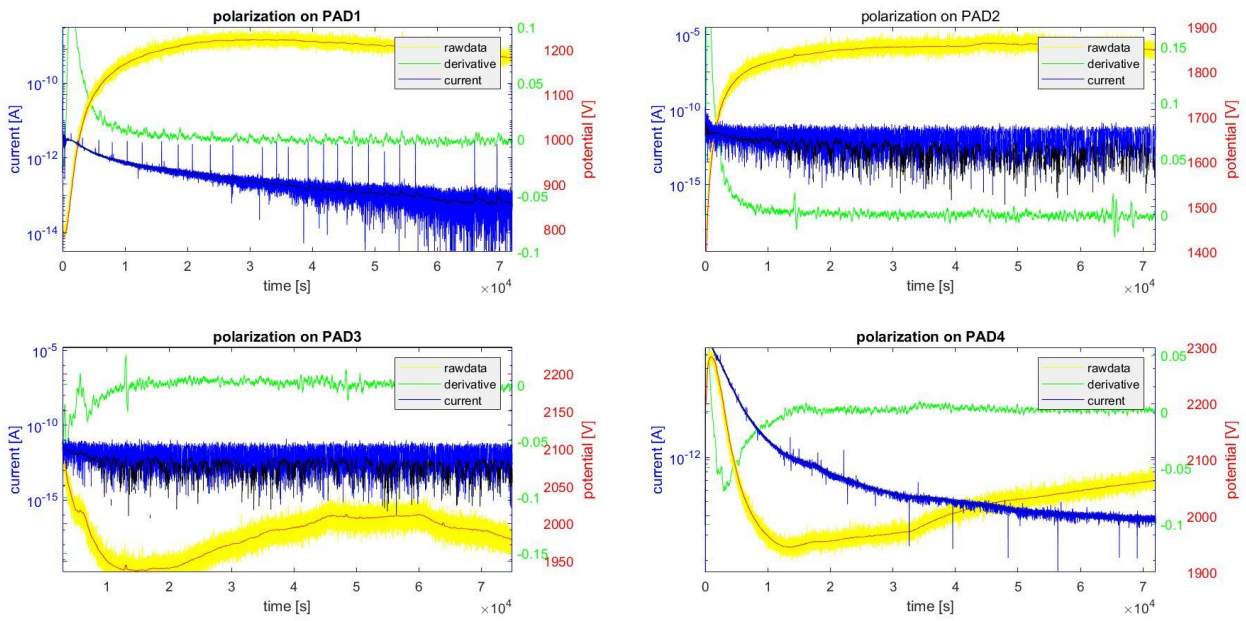


Figure 5-19 Polarization and current plots at 1 bar

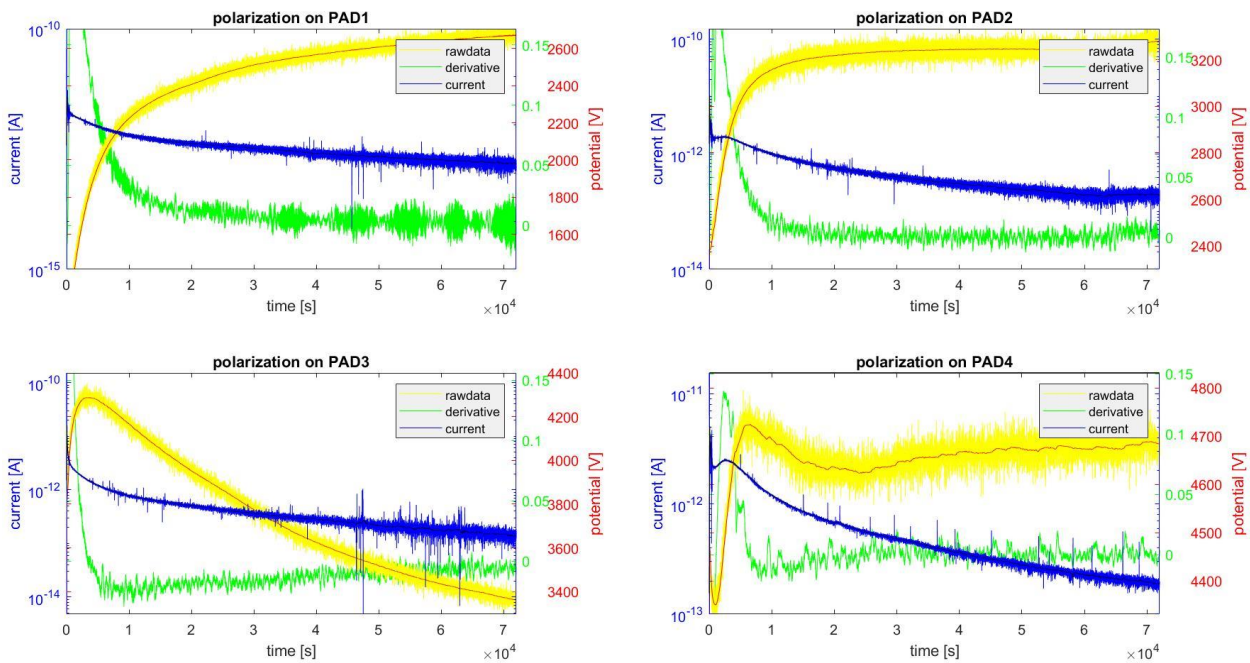


Figure 5-20 Polarization and current plots at 5 bar

It is useful to point out also that the data plotted in Figure 5-12, Figure 5-14, Figure 5-16 and in Figure 5-18, Figure 5-19, Figure 5-20 are the same, however in the last three figures different axis limits have been used to have a better view on the potential trends.

From these plots (especially in Figure 5-18) it can be clearly seen that current variations corresponds to potential variations on each pad, so it is clear that there is accumulated charge inside the specimen and that it affects the electric field distribution.

In many plots it can be noticed a variation of the potential after about 8 hours (between $2 \cdot 10^4$ and $4 \cdot 10^4$ seconds); this may suggest a new charge injection from the electrodes.

In pad 1 in Figure 5-19 the current plot presents some spikes; this happened probably due to an incorrect positioning of the HV terminal, that was too near to the metallic structure and that had some corona discharges outside from the specimen. In the same figure, there is a lot of noise in the current measurement on pads 2 and 3; this is due to an incorrect wire positioning (the HV terminal was in contact with the insulation of the ground wire). The noise has a very high intensity ($1 \cdot 10^{-10}$ A) and continues for the whole measurement hiding the real values.

None of these measurements presents any “step of death”, since the electric field used is very low (0.6 kV/mm), so it is very far from the breakdown electric field.

5.3.5 Electric field of all gaps

These plots compare the trends of the electric field (calculated as explained in section 5.2) of all gaps in polarization and depolarization. Without any charge accumulation all the plots should have a constant 0.6 kV/mm values, however the plotted values differ a lot from that.

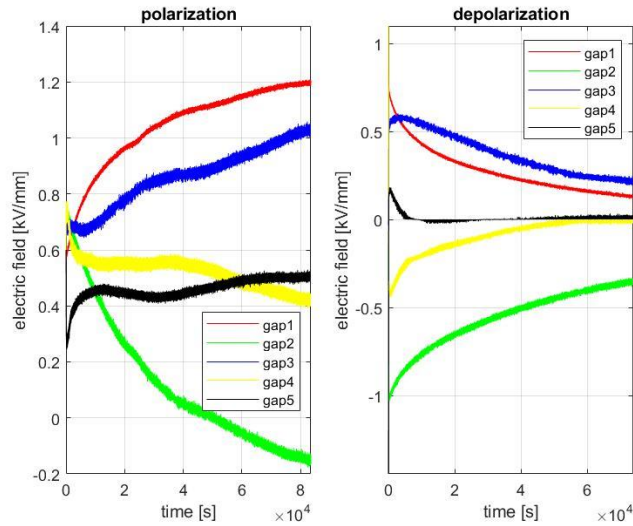


Figure 5-21 Electric field of all gaps at 0 bar

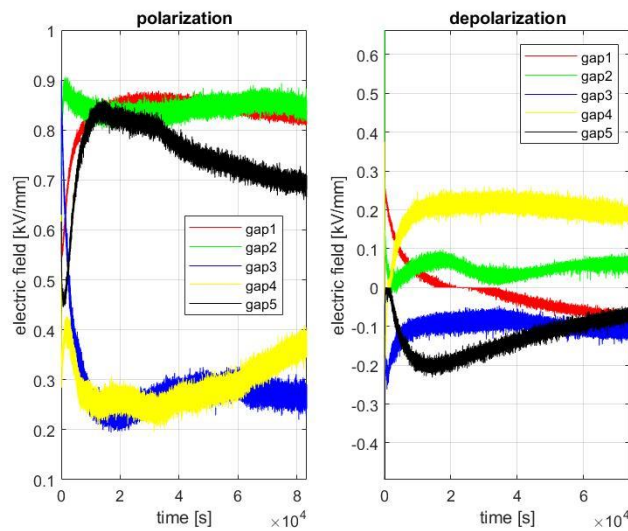


Figure 5-22 Electric field of all gaps at 1 bar

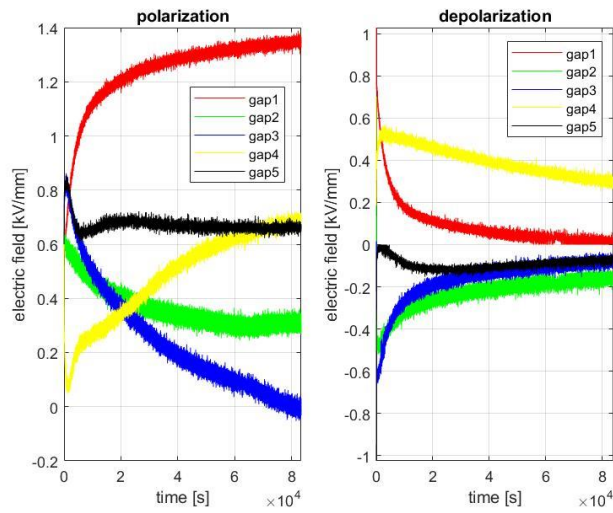


Figure 5-23 Electric field of all gaps at 5 bar

By comparing these figures, it can be noticed that the absolute value of the electric field in the gaps is higher at 0 and 5 bar than at 1 bar.

Another interesting thing that matches with previous observations is that at 1 bar (Figure 5-22) the maximum electric field is reached after almost 8 hours; this may justify a higher charge injection during that period.

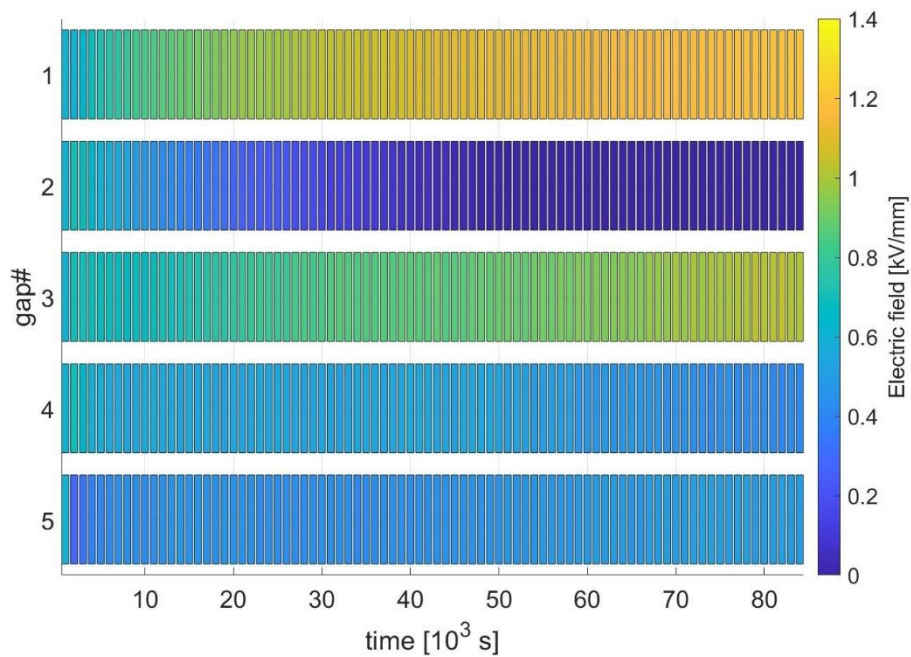


Figure 5-24 Electric field of all gaps at 0 bar

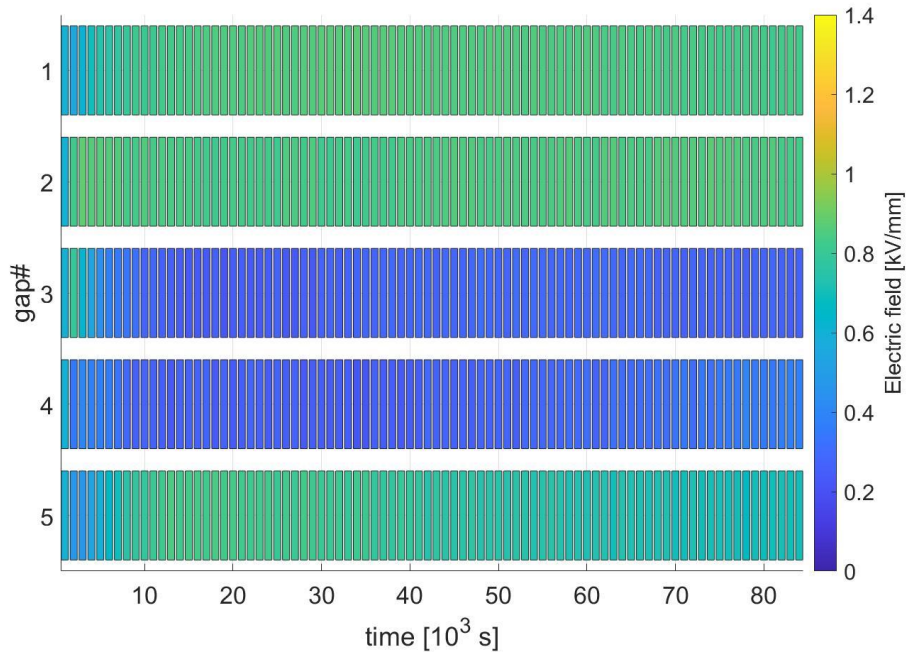


Figure 5-25 Electric field of all gaps at 1 bar

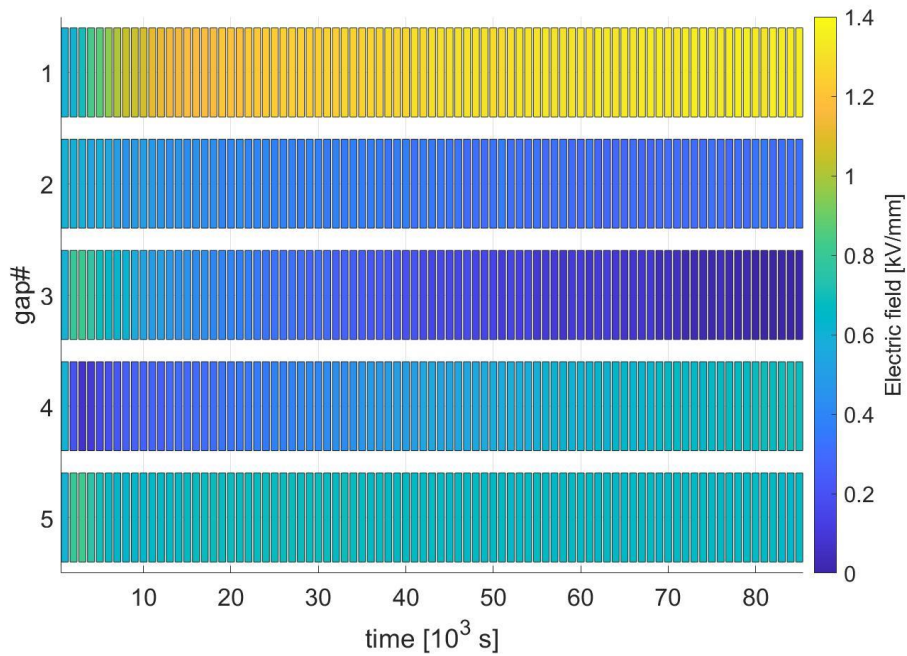


Figure 5-26 Electric field of all gaps at 5 bar

From these plots it can be noticed that gap 1 presents always a higher electric field than other pads, suggesting (like in section 5.3.2) a higher field distortion near the ground electrode.

5.3.6 Accumulated charge over each pad

These plots compare the trends of the accumulated charge in polarization and depolarization over each pad (these trends are calculated as explained in section 5.2).

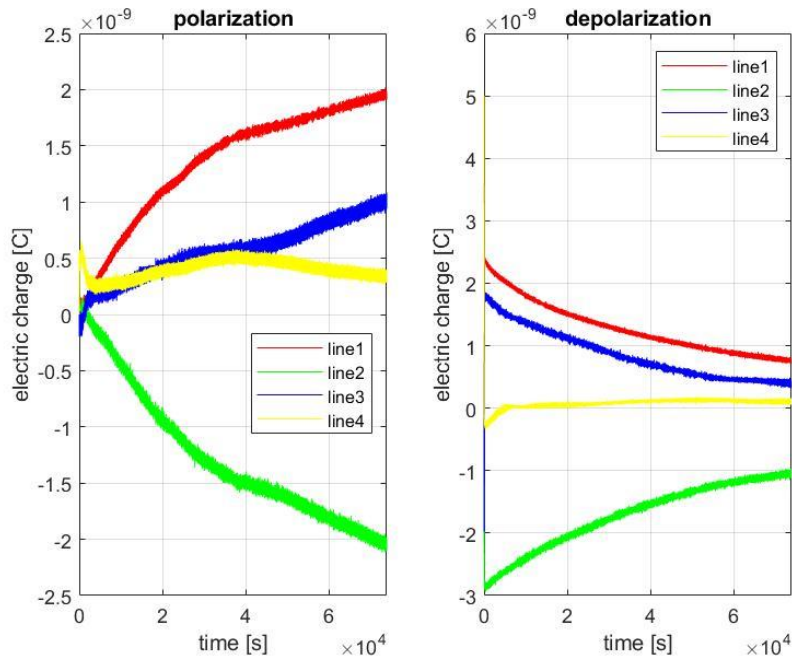


Figure 5-27 Electric charge distribution at 0 bar

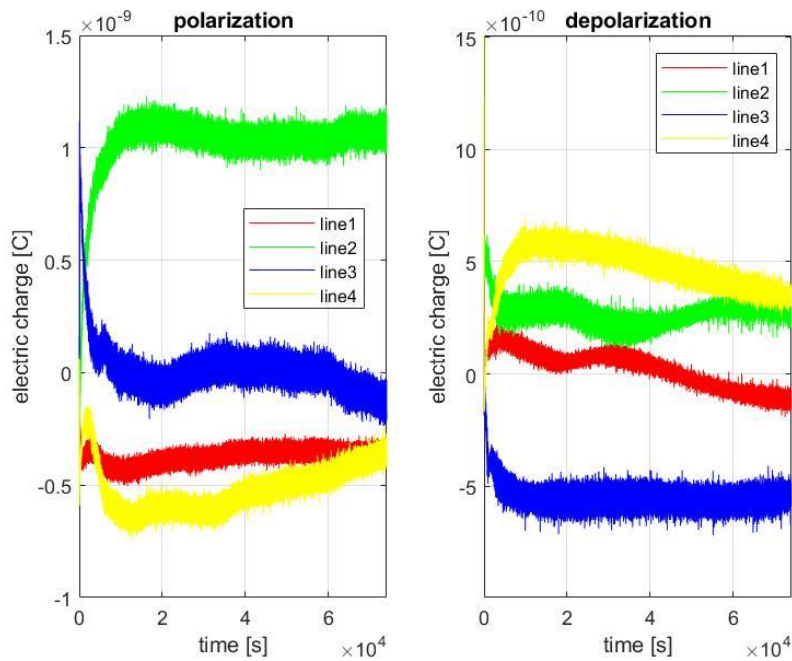


Figure 5-28 Electric charge distribution at 1 bar

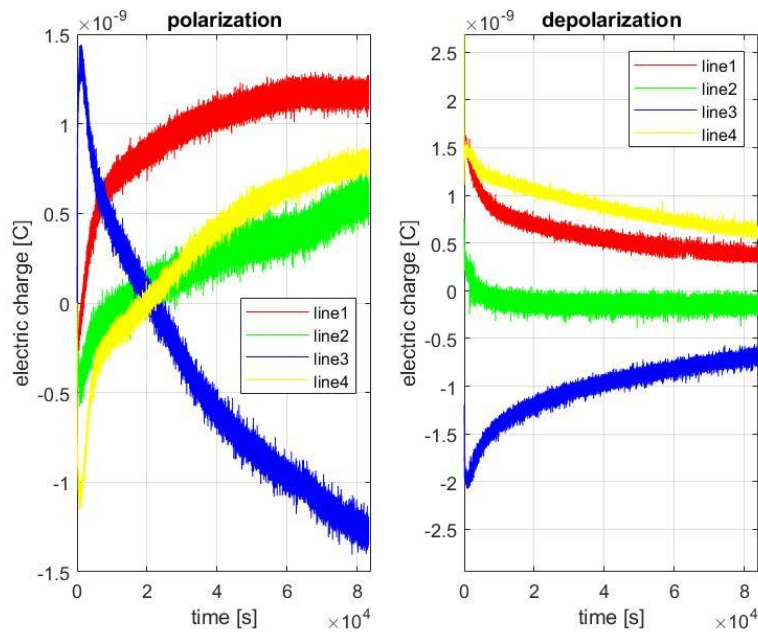


Figure 5-29 Electric charge distribution at 5 bar

As previously noted in section 5.3.2, also Figure 5-28 confirms that there is less accumulated charge at 1 and 5 bar than at 0 bar. This may be the reason why at 0 bar the breakdown voltages are lower than at higher pressures (Figure 4-21); however more measurements should be done in order to confirm this hypothesis.

As previously noted in section 5.3.4 between $2 \cdot 10^4$ s and $4 \cdot 10^4$ s the potential presents a change of steepness. Figure 5-27 shows that at 0 bar every charged line presents the same change in that same time interval.

There are some discrepancies between the last value of the polarization and the first of the depolarization; this may be due to the not uniform distribution of the electric field. Charge calculations here are done removing the contribution of the theoretical charge distribution due to a uniform field (since this electric field is generated by the power source). However, edge effects (see Figure 5-30, Figure 5-31 and Figure 5-32) influences the pad potential differently from the theoretical charge distribution considered, and this is the cause of such discrepancy. It must be noted that such discrepancy does not influence the validity of the trends shown and discussed here.

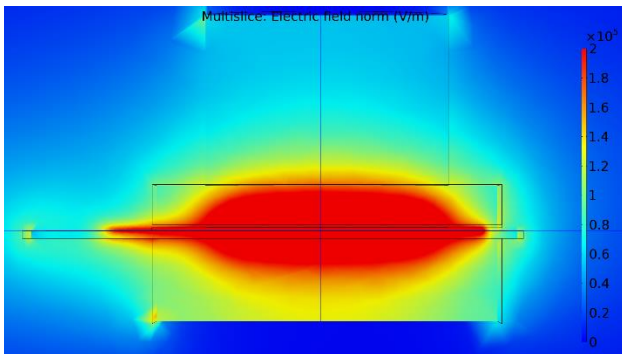


Figure 5-30 Electric field distribution (lateral view)

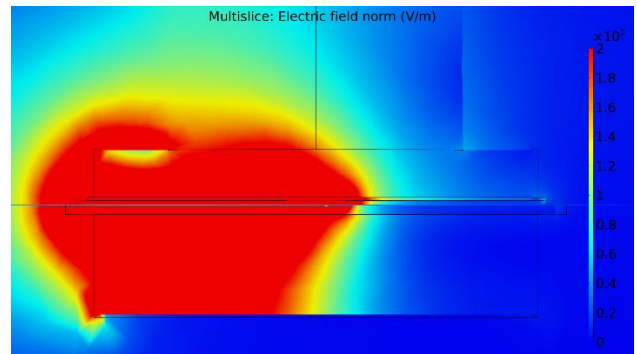


Figure 5-31 Electric field distribution (front view)

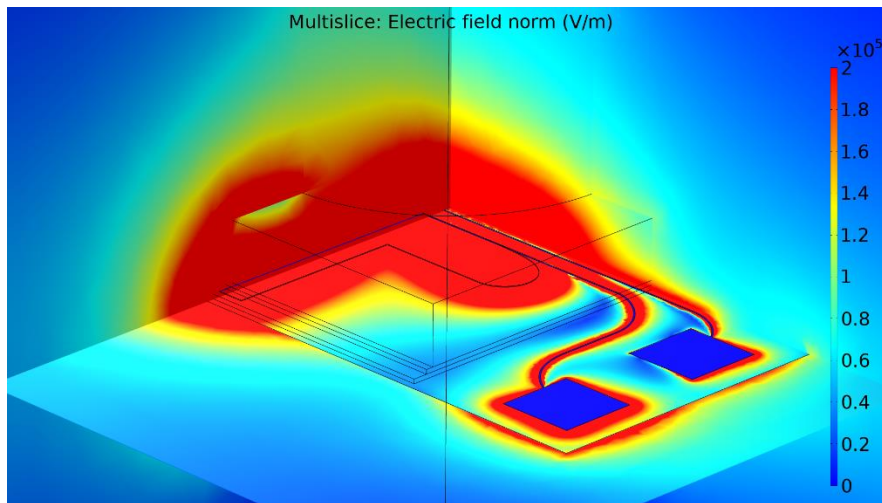


Figure 5-32 Electric field distribution

Chapter 6

Conclusions

Many factors are involved in the tangential electric field distribution at interface in HVDC joints; and nowadays no mathematical model can be found to represent it. In order to prevent joint failures and subsequent costs, it is fundamental to understand the breakdown mechanism to improve joint design and to find some diagnostic markers to prevent their breakdown.

By looking at the breakdown mechanism, Chapter 4 shows that no PDs were measured, thus the specimen's breakdown can't be imputed to them; therefore another mechanism must be involved in the specimen's breakdown. In section 0 it is shown how some hours before the breakdown there are anomalous current trends; this may indicate an electric charge movement inside the specimen or some new charge injection from the electrodes. The effect of accumulated charge is shown in Chapter 5, where it can be seen how much the injected electric charge can distort the internal electric field especially near the ground electrode. Another interesting observation is that the breakdown frequently happened in the middle of a voltage step, further suggesting that the accumulated charge is involved. From these observations it can be concluded that the phenomena that initiates the breakdown is strictly linked with the accumulated charge; however it is not sure if the failure of the dielectric is mostly due to the Coulomb forces developed in the material, or if it is due to high local electric fields achieved during charge redistribution at constant voltages.

Section 0 emphasizes how a possible diagnostic marker can be found in the increase of conductivity that often preannounced the breakdown of specimens. Such increase may be a step increase (as shown from Figure 4-30 to Figure 4-33) or a conductivity trend perturbation (as shown from Figure 4-34 to Figure 4-37). These events may be linked with charge accumulation inside the specimen and thus be linked with its breakdown, however this aspect should be further investigated.

From all the conductivity measurements carried out during this study, it can't be defined a clear dependency between the specimen's conductivity and the applied mechanical pressure. The attempts made to do so in Chapter 4 show that was not a possibility; this may be due to the aleatory nature of conductivity itself. In fact the conductivity of a single specimen depends on many variables, some of which linked to the manufacturing process. In order to define a general trend between conductivity and pressure, a more consistent and numerous statistical sample should be used.

Chapter 7

Narration of this work

This whole study has lasted exactly a year, during which many things happened and many mistakes were made but, by constantly adjusting the aim and the approach, we hit our target. I decided to add this chapter, which is just a narration of what happened during this year, to contextualize the obtained measurements and to illustrate all the thesis's pitfalls in order to demonstrate that it is more important to learn and go on, than to never fail.

It all began in November 2020 when I first got in the laboratory. Initially me and doctor Seri began by defining which types of specimens to use and how to make them: we had a sheet of already made "printed specimens", however we also decided to make the "sputtered" ones, in order to involve less factors in the study of the interface behaviour by eliminating the air gap variable. The very first masks used for the sputtered specimens were hand cut with a knife, however my cutting ability is not so good to perfectly reproduce a Rogowski profile, so the result was not satisfying. To overcome this problem, I also tried to use a 3D printer to make the masks (Figure 2-5, Figure 2-7) and it perfectly worked.

The first specimens were used to understand which was the maximum applicable electric field in order not to reach the breakdown and to protect the electrometer (this problem has later been overcome with the surge arrester in Figure 4-1). After this, we took our first measurements by applying from 1 to 4 kV for all the 4 different pressures on the specimens. This part has been very stressful because it has all been done manually; as a consequence, we realized that in order to reach better results (more precise and identical one to another) with a reasonable effort, it was necessary to automatize the process. This automatization also allowed us to apply higher voltages on the sample (otherwise I should have gone to the laboratory every 8 hours for weeks), therefore we became able to analyse what happened to the specimen before the breakdown. Doctor Seri specifically designed a DAC with an *Arduino nano*; the "*DACuino*" has an output voltage from 0 to 10 V and it is regulated via a *Matlab* script that allows the user to select the voltage, the step duration and many other features in order to control the voltage generator.

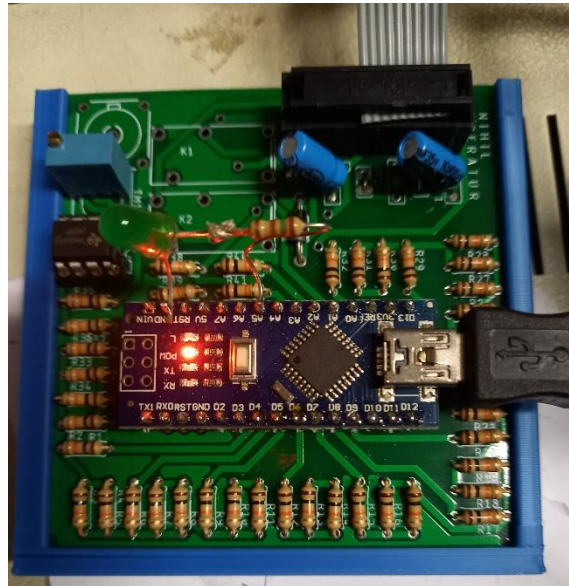


Figure 7-1 The DACuino

With the *DACuino* we started to take our first automatized current measurements: the applied voltage was from 1 to 20 kV in 8 hour steps with an amplitude of 1 kV (if the breakdown doesn't occur a measurement takes even one week). Later we also thought that a PD monitoring would have been essential to verify if the breakdown was due to the partial discharges or due to other causes. As for the PD monitoring, we initially used the *Techimp PDbase 2*, however it doesn't have an opensource system, therefore the instant of the occurrence of a partial discharge couldn't be seen. As a consequence, we switched to the *Tektronix* oscilloscope that, with a specifically designed *Matlab* code, was able to analyse the PDs on the TF^[7] map and to also send in output their ignition instant.

It was April 2021 when we had our first complete PD and current monitoring system in the way we wanted.



Figure 7-2 Laboratory

⁷ Time and Frequency plot

The first measurements showed hundreds of PDs and a perfect correlation between their occurrences and the current behaviour (Figure 7-3).

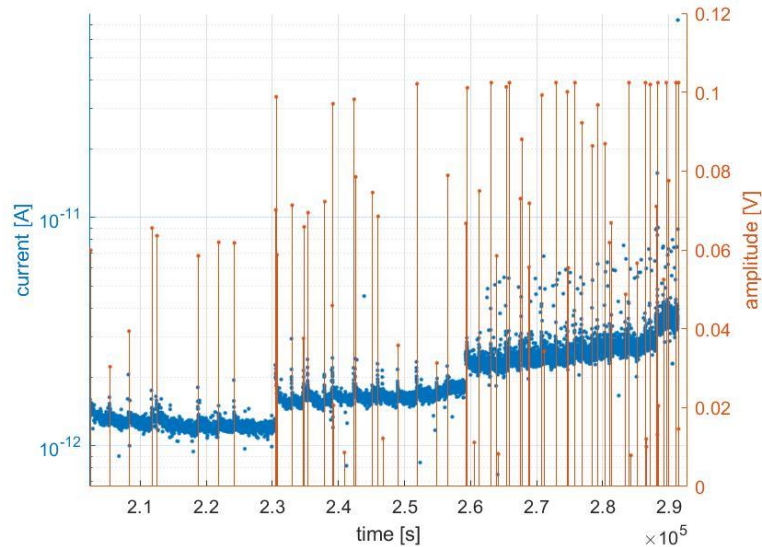


Figure 7-3 In blue the current value and in orange the occurrence of a PD

We started to think that the breakdown could be linked to the partial discharges, so many *Matlab* scripts were designed to analyse the PDs and all the measurements for the four pressures (both for the sputtered and the printed specimens) were taken.

However a day of June 2021, I went to the laboratory to collect the last measurement and when I opened the PTFE press I noticed some burns on it.

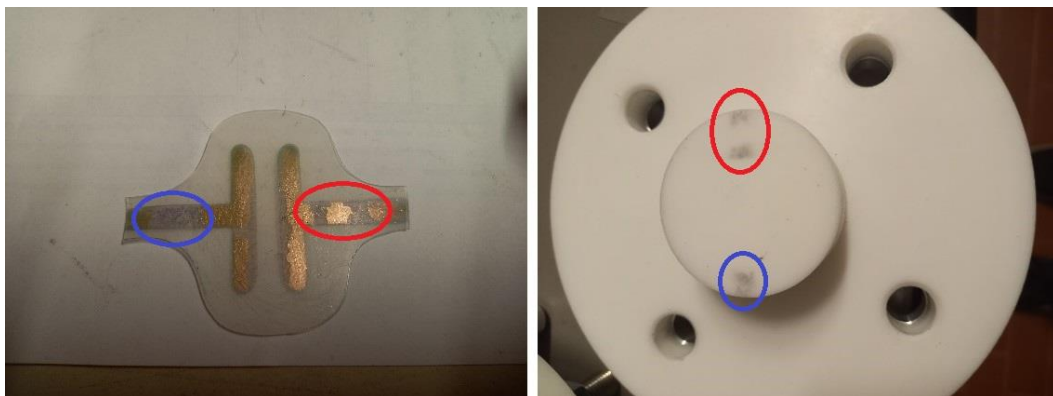


Figure 7-4 Burns on the PTFE structure

It was a clear sign that the partial discharges were not happening inside the specimen but between the specimen and the press! We run some simulation on *COMSOL* and we obtained the confirm to our suspects, the electric field between the PTFE and the specimen was too high. We took a few other measurements with the long backing and no partial discharges were shown! It was the end of June

when I realized that, in order to show clear results, I should have done all the measurements made till then again (this time using a long backing). It was due to this problem that I didn't proceed any further with the printed specimens measurements (there was no time to retake also those measurements) so we focused only on the sputtered ones. After that inconvenient, the initial hypothesis of a breakdown due to the Coulomb force pulling the accumulate space charge was back in the game, so we started the space charge measurements session.

During these measurements we connected the *Trek electrostatic voltmeter* to an *Arduino due* to convert the output and to send it to a PC through a serial port; this has been fundamental to obtain the trend of the pads potential through time. Fortunately, this time nothing weird happened (except for a little problem with the *Arduino* converter, that has been immediately solved) and at the end of October, all the measurements were ready.

In conclusion it has been a very long year, full of mistakes but also full of good results. I am very happy to have chosen this thesis because it taught me how to correctly approach a scientific research and to always look at every little detail of the chosen approach.

Acknowledgements

Foremost, I would like to acknowledge professor Cavallini and doctor Seri to have given me the opportunity to work on this very actual and interesting topic; in particular I want to thank professor Seri that has made this thesis possible with all his *Arduino* projects and that helped me a lot with all the thesis work.

Another thanks goes to Leonardo and to all the other members of the LIMES, that helped me through many of the issues faced in the laboratory and that warmly welcomed me in their group. I have never felt alone in the lab and all of you have always been very helpful to me, thank you all.

I would also thank my best friend Tommi that in these years has been an excellent adventures partner and that always tried to motivate and challenge me in many aspects of my studies and personal life. If it wasn't for you, I would not have done so many things in my life, so thank you.

A very important thanks goes to my Piccioni (Dozza, Gerald, Ge, Luci, Marti, Ponzio, Raymed), that remind me every day that in life there are many highs and lows, but a true bond goes through every difficulty.

Another thanks goes to the best study group ever, thank you Fillo, Gabbo and Stumpo for making the study period during the lockdown more cheerful.

Finally, I would also thank the E.N.B. for all the experiences and emotions that have been offered to me in this period, because even if it has been very short, it has been enough to make me feel part of it.

Furthermore, I would also like to point out that this thesis is not the conclusion of my studies, but it is just the starting milestone of a long and difficult path that I will follow for the rest of my life.

In conclusion, I dedicate all the effort and fatigue spent in these five years to all of my friends that have always been kind, supportive and that have always been able to understand my choices; I owe you a lot.

Acronyms

HVDC = High Voltage Direct Current

PD = Partial Discharges

AC = Alternating Current

DC = Direct Current

HV = High Voltage

GND = Ground

BD = Breakdown

DAC = Digital to Analog Converter

PCB = Printed Circuit Board

HFCT = High Frequency Current Transformer

XLPE = Cross-linked Polyethylene

PTFE = Polytetrafluoroethylene

PMMA = Polymethylmethacrylate

Bibliography

- [1] Recommendations to improve HVDC cable systems reliability (joint entsoe and europacable paper).
- [2] Hui, B.: 'Fault Statistics and Typical Case Analysis of High Voltage Cable System', China Society of Electrical Engineering Annual Meeting, 2017.
- [3] Ye, Hanyu, et al. Review on HVDC cable terminations. *High voltage*, 2018, 3.2: 79-89.
- [4] Mazzanti G. et al. The insulation of HVDC extruded cable system joints. Part 1: review of materials, design and testing procedures. *IEEE Transactions on Dielectrics and Electrical Insulation*, 2019, 26.3: 964-972.
- [5] Ruben Vogelsang, Hans-Jörg Winter, Hansjörg Gramespacher, Martin Grunwald, „Silicone technology for reliable performance of joints and terminations for high voltage polymer power cables”, 8th International Conference on Insulated Power Cables, Versailles, France, 2011.
- [6] ZHU, Bin, et al. Relationship between the interfacial ramped DC breakdown voltage and the morphology of the XLPE/SiR interface. *IEEE Transactions on Dielectrics and Electrical Insulation*, 2019, 26.3: 689-697.
- [7] GREENWOOD, James A.; WILLIAMSON, JB Pl. Contact of nominally flat surfaces. *Proceedings of the royal society of London. Series A. Mathematical and physical sciences*, 1966, 295.1442: 300-319.
- [8] Jeroense, M., Saltzer, M., Ghorbani, H.: 'Technical challenges linked to HVDC cable development', *ABB Review*, 2013
- [9] Fälth, Fredrik, Santhosh Kumar, and Hossein Ghorbani. "Robustness analysis of classical high voltage joint design under high voltage DC stress." *Proceedings of the Nordic Insulation Symposium*. No. 23. 2013.
- [10] Ye, Hanyu, et al. Design aspects on HVDC cable joints. In: 2018 12th International Conference on the Properties and Applications of Dielectric Materials (ICPADM). IEEE, 2018. p. 300-304.
- [11] Frobin, Saskia Josefine, et al. "A Generic Approach for HVDC Cable Accessories Modelling." 2018 IEEE 2nd International Conference on Dielectrics (ICD). IEEE, 2018.
- [12] TRINH, N. Giao. Electrode design for testing in uniform field gaps. *IEEE Transactions on Power Apparatus and Systems*, 1980, 3: 1235-1242.
- [13] Tornichi Torque Handbook Vol.9